Journal of Alzheimer's Disease 55 (2017) 391–410
DOI 10.3233/JAD-160051
IOS Press

Cyclic *cis*-Locked Phospho-Dipeptides Reduce Entry of AβPP into Amyloidogenic Processing Pathway

Carolyn L. Fisher[a], Ross J. Resnick[a], Soumya De[b], Lucila A. Acevedo[a], Kun Ping Lu[c], Frank C. Schroeder[d] and Linda K. Nicholson[a,*]
[a]*Department of Molecular Biology & Genetics, Cornell University, Ithaca, NY, USA*
[b]*School of Bio Science, Indian Institute of Technology, Kharagpur, WB, India*
[c]*Department of Medicine, Division of Translational Therapeutics, Beth Israel Deaconess Medical Center, Harvard Medical School, Boston, MA, USA*
[d]*Boyce Thompson Institute, Cornell University, Ithaca, NY, USA*

Accepted 10 August 2016

Abstract. The *cis*/*trans* isomerization of X-Pro peptide bonds in proteins in some instances acts as a molecular switch in biological pathways. Our prior work suggests that the *cis* isomer of the phospho-Thr668-Pro669 motif, located in the cytoplasmic domain of the amyloid-β protein precursor (AβPP), is correlated with an increase in amyloidogenic processing of AβPP and production of amyloid-beta (Aβ), the neurotoxic peptide fragment in Alzheimer's disease (AD). We designed a 100% *cis*-locked cyclic dipeptide composed of cyclized phospho-Thr-Pro (pCDP) as a mimic for this putative pathological conformation, and three phosphate-blocked derivatives (pCDP-diBzl, pCDP-Bzl, and pCDP-diPOM). Two H4 neuroglioma cell lines were established as AD cell models for use in testing these compounds: H4-AβPP695 for stable overexpression of wild-type AβPP695, and H4-BACE1 for stable overexpression of β-site AβPP cleaving enzyme-1 (BACE1). The level of the secreted AβPP fragment resulting from BACE1 activity, sAβPPβ, served as a key proxy for amyloidogenic processing, since cleavage of AβPP by BACE1 is a requisite first step in Aβ production. Of the compounds tested, pCDP-diBzl decreased sAβPPβ levels in both cell lines, while pCDP-diPOM decreased sAβPPβ levels in only H4-BACE1 cells, all with similar dose-dependences and patterns of proteolytic AβPP fragments. Enzymatic assays showed that none of the pCDP derivatives directly inhibit BACE1 catalytic activity. These results suggest a model in which pCDP-diBzl and pCDP-diPOM act at a common point to inhibit entry of AβPP into the amyloidogenic AβPP processing pathway but through different targets, and provide important insights for the development of novel AD therapeutics.

Keywords: Alzheimer's disease, amyloid beta-protein precursor, cyclic dipeptides, diketopiperazine, phosphorylated Thr668

INTRODUCTION

Cyclic dipeptides (CDPs) are 2,5-diketopiperazine structures that are naturally abundant across all organisms, including mammals [1–4]. The core CDP structure, with backbone hydrogen bond donors and acceptors, can easily bind to catalytic and regulatory sites within enzymes [2]. CDPs can be synthesized under physiological conditions using mild acid or base chemistry [2, 5], which is the process by which cyclic-His-Pro is produced in mammalian nervous systems [6]. Specific CDPs act as kinase antagonists [7], chitinase inhibitors [8], cancer drugs that cause apoptosis and growth inhibition of HT-29 colon cancer tumor cells [9], and neuroprotective agents in rats with impaired motor and cognitive abilities [10].

*Correspondence to: Linda K. Nicholson, Department of Molecular Biology & Genetics, Cornell University, Ithaca, NY 14853, USA. Tel.: +1 607 255 7208; Fax: +1 607 255 6249; E-mail: lkn2@cornell.edu.

Although the exact mechanism of action for these neuroprotective CDPs is not well understood, there is evidence suggesting that increased astrocyte activity, decreased caspase-3, or reduced microglial reactivity could explain the neuroprotective properties of certain CDPs (reviewed in [3]). CDPs are generally small (<500 Da) and can diffuse through membranes, the blood-brain barrier, and can often be taken up by peptide transporters [2]. Despite their reported neuroprotective effects, the extent to which CDPs affect the production of Aβ peptide, the neurotoxic peptide fragment upregulated in Alzheimer's disease (AD) pathology, has not been tested.

The amyloid-β protein precursor (AβPP) is involved in a variety of cellular processes connected to the pathogenesis of AD [11]. AβPP is a type 1 transmembrane protein composed of a large N-terminal extracellular domain, a single α-helix transmembrane domain, and a cytoplasmic tail (Fig. 1A) [12]. AβPP is proteolytically cleaved *in vivo* in two ways by the cell (reviewed in [13]), depending on its cellular localization. At the plasma membrane, AβPP is dominantly processed via the nonamyloidogenic pathway. Here, α-secretases constitutively cleave AβPP into sAβPPα and C83 fragments [14]. C83 is further cleaved by γ-secretase producing p3 and AβPP intracellular domain (AICD). Alternatively, in the amyloidogenic pathway, AβPP can be internalized and localized to endosomes, where β-secretase (β-site AβPP cleaving enzyme 1, or BACE1) cleaves AβPP to produce sAβPPβ and C99 fragments [15], followed by γ-secretase cleavage of C99 to produce neurotoxic Aβ peptide and AICD (Fig. 1A).

The innate balance between nonamyloidogenic and amyloidogenic AβPP processing can be shifted by a number of factors. Cleavage of AβPP by BACE1 is enhanced by elevated BACE1 expression [16], by elevated AβPP gene dosage such as in trisomy 21 individuals [17, 18], by familial AβPP mutations [19], and by cholesterol enrichment in membrane invaginations (reviewed in [20]). Conversely, a BACE1 cleavage site mutation in AβPP identified in an Icelandic population has been found to be protective against AD [21]. In cells, this mutation reduces BACE1-mediated AβPP cleavage and shifts AβPP processing away from the amyloidogenic route [21]. Other genetic changes that protect against AD include the E2 allele of the apolipoprotein E (APOE) [22, 23] and the BACE1-knockout, which has been shown to abolish AD pathology in mice [24]. Clearly, the regulation of AβPP processing is complex, and the development of chemical probes that alter AβPP processing could serve as useful tools for the development of strategies to prevent and/or treat AD.

Within the cytoplasmic tail of AβPP (AβPPc), the level of phosphorylation of the Thr668-Pro669 (TP) motif (Fig. 1B) is increased in the AD brains [25] and may be an important signaling motif that becomes dysregulated in the development of AD [25–27]. Prior to phosphorylation, the *trans*-isomer of the TP peptide bond is stabilized by the formation of a helix-capping box structure [28] (Fig. 1A, pink box) and no *cis*-TP isomer is detected [29]. Only after phosphorylation is the helix-capping box destabilized (Fig. 1B) and a *cis*-phosphorylated-TP (pTP) population emerges in ∼10% abundance with the *trans*-pTP isomer in ∼90% abundance [29]. The exchange between *cis* and *trans* isomers of the pTP peptide bond is very slow [30], and is accelerated by ∼2000 fold by the enzyme Pin1 [27, 31]. Additionally, brain tissue from Pin1 knockout mice show an increase in the phosphorylation of Thr668 in AβPP and in amyloidogenic AβPP processing (Fig. 1A) [32]. Since pThr668 accumulates in AD brains [25] and is required for formation of the *cis*-pTP isomer [29], the *cis* isomer might serve as a molecular signal for putative cellular binding proteins that localize AβPP to endosomes for β-secretase cleavage.

To test the importance of the *cis*-pTP conformation as a signal for AβPP processing, we synthesized a small molecule, phospho-Thr-Pro cyclic dipeptide (pCDP) (Fig. 1C), that is a 100% "*cis*-locked" mimic of the *cis*-pTP motif in the AβPP cytoplasmic tail. Three additional pCDP derivatives with blocking groups on the phosphate moiety were generated to test delivery and activity of these molecules in cells (Fig. 2). Two distinct H4 neuroglioma cell lines that stably overexpress either AβPP695 (H4-AβPP695) or BACE1 (H4-BACE1) were generated, providing AD cell models in which the effects of pCDP compounds on AβPP processing production were investigated. The secreted product of AβPP cleavage by BACE1, sAβPPβ, was used as a proxy for monitoring amyloidogenic processing. Testing of pCDPs in two comparative AD models revealed that, while both pCDP-diBzl and pCDP-diPOM inhibit amyloidogenic AβPP processing, they must act through different targets but at a similar point in the pathway. Together, these data suggest that pCDP-diBzl and pCDP-diPOM molecules provide intriguing tools for investigating the role of *cis*-pTP conformation in the proteolytic processing of AβPP, potentially leading to novel strategies for inhibiting the production of Aβ.

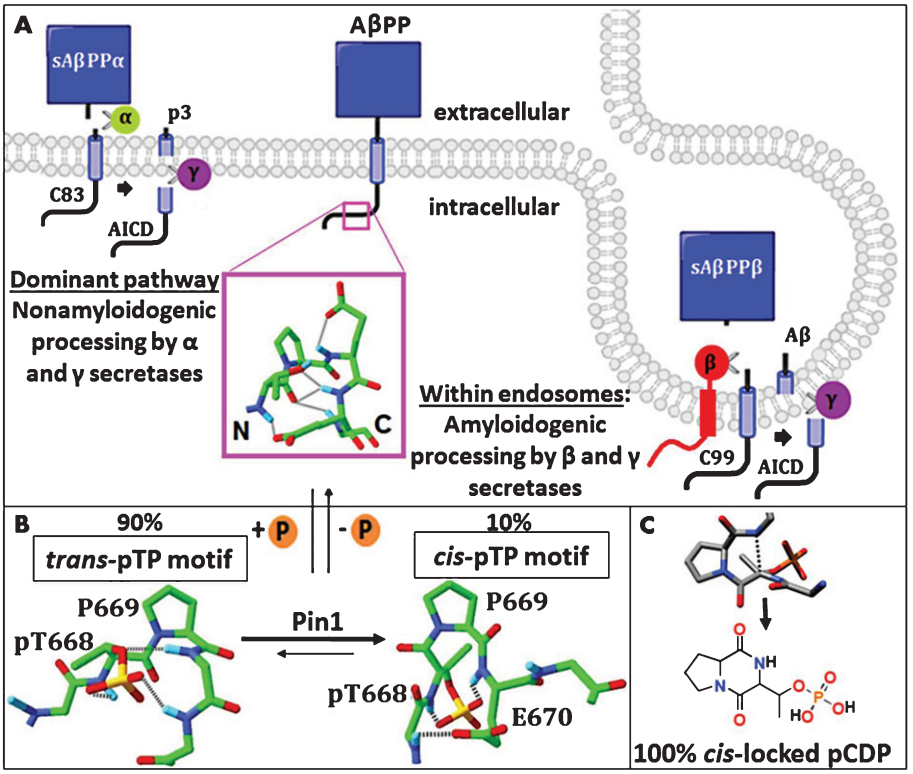

Fig. 1. Putative role of the phospho-Thr668-P669 *cis* isomer as a signal in the proteolytic processing of AβPP. A) AβPP is a type 1 transmembrane protein with a large N-terminal ectodomain and a short C-terminal cytoplasmic tail. At the plasma membrane, α and γ secretases are abundant to cleave AβPP into sAβPPα, C83, p3, and AICD fragments in the dominant, nonamyloidogenic processing pathway. AβPP can alternatively be internalized and localized to acidic compartments where BACE1 (β-secretase) and γ-secretase cleave AβPP into sAβPPβ, C99, Aβ, and AICD fragments via amyloidogenic processing. Within the cytoplasmic tail of AβPP, the amino acids T668-P669-E670-E671 form a transient helix capping box (pink box, A). Upon phosphorylation of T668, the helix-capping box is destabilized and two different structures emerge (B). These two structures are distinguished by their *cis* versus *trans* isomer state of the pT668-P669 peptide bond. Pin1 has been identified as a peptidyl prolyl isomerase that rapidly establishes the equilibrium concentrations of 90% *trans*-pTP and 10% *cis*-pTP. By creating a covalent bond between the α-carbon of the T668 and the amine of the E670, a "100% *cis*-locked" phosphorylated cyclic-dipeptide (pCDP) was generated to mimic the *cis*-pTP motif (C).

MATERIALS AND METHODS

Materials

The human H4 neuroglioma cell line was purchased from ATCC (Manassas, VA). Dulbecco's Modified Eagle Medium (DMEM), Penicillin-Streptomycin and culture dishes were from Corning Life Sciences (Tewksbury, MA); Fetal bovine serum (Premium Select) was purchased from Atlanta Biologicals (Flowery Branch, GA); DC Protein Assay Kit, Pre-stained Dual Color Protein Standards, Clarity Western ECL, Chemidoc MP System, Image Lab Software, Chemi Hi Sensitivity blot application, Immuno-Blot LF PVDF membrane, 4–20% Mini Protean TGX Stain Free precast gels, and 4–15% Mini Protean TGX Stain Free precast gels were obtained from BioRad (Hercules, CA); polyvinylidene fluoride (PVDF) transfer membrane (0.45 mm) was purchased from Perkin Elmer (Waltham, MA); Whatman nitro-cellulose transfer membrane (0.2 μm) was purchased from GE Healthcare Life Sciences; Lipofectamine 2000, Pierce ECL Western Blotting, Pierce SuperSignal West Pico substrates and G418 sulfate (Geneticin) were all from ThermoFisher Scientific (Waltham, MA); Recombinant Human BACE1 protein, CF (931-AS) and Mca-SEVNLDAEFRK(Dnp)RR-NH2 Fluorogenic Peptide Substrate (ES004) were acquired from R&D Systems (Minneapolis, MN); the BACE1 inhibitor LY2811376 was purchased from Selleckchem (Houston, TX).

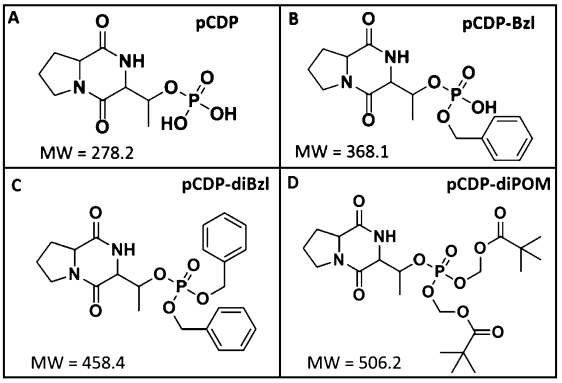

Fig. 2. The *cis*-locked pCDP mimic was derivatized to aid in more favorable cellular uptake. Chemical structure variations of the *cis*-locked pCDP mimic, shown in (A), include the attachment of one benzyl (Bzl) group to produce pCDP-Bzl (B), two benzyl groups (diBzl) to produce pCDP-diBzl (C), or two pivaloyloxymethyl (POM) groups to produce pCDP-diPOM (D). Molecules generated using ChemDraw 15.0.

Plasmids

pCAX-AβPP^{695} expressing full-length human AβPP695 was a gift from Dennis Selkoe and Tracy Young-Pearse (Addgene plasmid # 30137). pCMV6-XL5-BACE1 expressing full-length human BACE1, transcript variant a, NM_012104.3 (# SC115547) was purchased from Origene, Rockville, MD. pSV2neo [33] which provides a selectable marker for resistance to the antibiotic G418 in mammalian cell lines was a gift from David Shalloway, Cornell University.

Antibodies

Rabbit anti-sAβPPβ (poly8134, 813401) and the mouse monoclonal antibody 6E10 (803001) were purchased from BioLegend (San Diego, CA) and the anti-β-tubulin mouse monoclonal antibody (2G7D4, A01717-40) was acquired from GenScript (Piscataway, NJ). The rabbit monoclonal antibodies anti-AβPP (EPR5119(2), ab133588), anti-C-terminal AβPP antibody Y188 (ab32136) and anti-BACE1 (EPR3956, ab108394) were all purchased from Abcam (Cambridge, MA). Goat anti-rabbit and goat anti-mouse horseradish peroxidase (HRP)-conjugated secondary antibodies were from Jackson ImmunoResearch Laboratories (West Grove, PA). The anti-pan-Aβ rabbit monoclonal antibody (D54D2) was purchased from Cell Signaling Technology (Danvers MA).

Cell culture

All H4 neuroglioma cell lines were routinely grown in monolayer culture in growth medium consisting of DMEM (4.5 g/L glucose, 3.7 g/L sodium bicarbonate) supplemented with 10% fetal bovine serum and 100 IU /100 μg/mL penicillin/streptomycin at 37°C in a humidified atmosphere (90%) containing 10% CO_2. Cells were isolated by trypsinization and routinely passaged to maintain stocks or plated for experiments as described below or in the figure legends.

Generation of H4 neuroglioma cell lines overexpressing AβPP^{695} or BACE1

Cell lines constitutively over-expressing human AβPP^{695} (H4-AβPP695) or human BACE1 (H4-BACE1) were created by co-transfecting either pCAX-AβPP^{695} or pCMV6-XL5-BACE1 (2–4 μg) with the G418 resistance plasmid pSV2neo (0.2–0.4 μg) into H4 neuroglioma cells using Lipofectamine 2000 according to the manufacturer's instructions. Forty-eight hours after transfection, cells were split into growth medium supplemented with 500 μg/mL of G418 and after 2-3 weeks G418 resistant colonies were screened by immunoblotting for AβPP or BACE1 over-expression as compared to the parental H4 cell line. Positive clones were expanded and maintained in growth medium containing 200 μg/mL G418 until frozen.

Analysis of custom-synthesized compounds

Nuclear magnetic resonance (NMR) analysis: All pCDPs used in this study (pCDP, pCDP-Bzl, pCDP-diBzl, pCDP-diPOM) were custom synthesized using green chemistry [34] and phosphorylation of Threonine completed [35, 36] by Viva Biotech Ltd. (Shanghai, China) and purchased through Trillience (Toronto, Ontario). Deuterated-methanol NMR solvent (99.8%, CD3OD) was purchased from Cambridge Isotope Laboratories and used for each sample preparation. NMR spectra (1H and 13C) were recorded at room temperature (RT) with a Bruker Avance^{III} HD 800 MHz instrument (SUNY-ESF) or a Varian Inova 600 MHz instrument (Cornell University). Chemical shifts are reported in δ (ppm) units relative to residual solvent peaks CD3OD (3.31 ppm for 1H, 49.0 ppm for 13C). Splitting patterns are assigned as s (singlet), d (doublet), t (triplet), q (quartet), p (pentet), m (multiplet), dd (doublet of

doublets), ddd (doublet of doublet of doublets), dddd (doublet of doublet of doublet of doublets), dq (doublet of quartets), dt (doublet of triplets), td (triplet of doublets), qd (quartet of doublets), and pd (pentet of doublets). All NMR spectra were analyzed with MNOVA software (v.10.0). Supplementary Figures 1–4 show 1H NMR spectra for the pCDP compounds.

Liquid chromatography mass spectrometry (LCMS) analysis: Each pCDP standard sample was diluted from 100 mM of stock pCDP in dimethyl sulfoxide (DMSO) down to 1 μM pCDP in 1:1 methanol/water and 2 μL was separated using reverse-phase high resolution UHPLC-MS with an Agilent Zorbax RRHD Eclipse XDB-C18 column (2.1 × 100 mm, 1.8 μm particle diameter), 0.1% formic acid in acetonitrile (organic phase), and 0.1% formic acid in water (aqueous phase) at a rate of 0.5 mL/min for 15 min at 40°C (through the Chromelon Xpress software system) on a Thermo Scientific Dionex Ultimate3000 UHPLC system, equipped with a diode array detector and connected to a Thermo-Scientific Q Exactive hybrid quadupole-Orbitrap mass spectrometer (Boyce Thompson Institute Mass Spectrometry Center, Cornell University). A solvent gradient scheme was used: 5% organic for 1.5 min, a linear increase to 100% organic over 11 min, and then a 2-min hold at 100% organic before decreasing back to 5% organic over 0.1 min with a final hold at 5% organic for the last 0.4 min, for a total of 15 min. The Thermo-Scientific Xcalibur software package was used to visualize, analyze, and depict the LCMS data shown in Supplementary Figure 5.

pCDP (Supplementary Figures 1 and 5A)

1H NMR (800 MHz, CD3OD, 25°C): δ 1.53 (d, J = 6.5 Hz, 3H), 1.90–1.96 (m, 1H) 1.98–2.04 (m, 2H), 2.28–2.34 (m, 1H), 3.45 (ddd, J = 11.9, 9.1, 3.0Hz, 1H), 3.65 (dt, J = 11.6, 7.9, 1H), 4.12 (dt, J = 3.4, 1.6Hz, 1H), 4.22 (ddd, J = 9.8, 6.8, 1.7Hz, 1H). 13C NMR (800 MHz, CD3OD, 25°C): δ 19.01, 22.85, 29.10, 46.02, 60.64, 59.89, 72.91, 165.82, 171.71. HR-LCMS (ESI+): Calculated C9H15N2O6P + [M + H]+ = 279.07471; found [M + H]+ = 279.07360, mass tolerance 0.1 mmu, retention time = 1.12 min.

pCDP-Bzl (Supplementary Figures 2 and 5B)

1H NMR (600 MHz, CD3OD, 25°C): δ 1.52 (d, J = 6.3 Hz, 3H), 1.84–1.96 (m, 2H), 1.97–2.07 (m, 1H), 2.22–2.30 (m, 1H), 3.39 (ddd, J = 11.9, 8.7, 3.7 Hz, 1H), 3.49 (dt, J = 11.7, 8.2 Hz, 1H), 4.02 (d, J = 5.9 Hz, 1H), 4.18 (dd, J = 8.1, 8.3 Hz, 1H), 4.73 (dt, J = 7.4, 6.1 Hz, 1H), 4.92 (d, J = 6.2 Hz, 2H), 7.24 (t, J = 7.3 Hz, 1H), 7.31 (t, J = 7.6 Hz, 2H), 7.40 (d, J = 7.4 Hz, 2H). 13C NMR (800 MHz, CD3OD, 25°C): δ 19.41, 22.98, 28.95, 45.96, 59.91, 60.73, 68.55, 71.95, 128.12 (2C), 128.49, 129.09 (2C), 139.15, 166.04, 171.84. HR-LCMS (ESI+): Calculated C16H21N2O6P + [M + H]+ = 369.12166; found [M + H]+ = 369.12050, mass tolerance 0.5 mmu, retention time = 4.43 min.

pCDP-diBzl (Supplementary Figures 3 and 5C)

1H NMR (800 MHz, CD3OD, 25°C): δ 1.51 (d, J = 6.8 Hz, 3H), 1.82 (m, 3H), 2.26 (m, 1H), 3.38 (m, 2H), 4.17 (m, 2H), 5.03 (m, 4H), 5.27 (pd, J = 1.8, 6.8 Hz, 1H), 7.35 (m, 10H). 13C NMR (800 MHz, CD3OD, 25°C): δ 18.57, 22.98, 29,58, 46.24, 60.08, 60.95, 70.60, 70.81, 75.08, 128.91 (3C), 129.11 (3C), 129.60, 129.65, 129.66, 129.68, 137.32 (2C), 164.96, 171.66. HR-LCMS (ESI+): Calculated C23H27N2O6P + [M + H]+ = 459.16861; found [M + H]+ = 459.16706, mass tolerance 0.1 mmu, retention time = 7.49 min.

pCDP-diPOM (Supplementary Figures 4 and 5D)

1H NMR (800 MHz, CD3OD, 25C): δ 1.25 (d, J = 2.5 Hz, 18H), 1.58 (d, J = 6.8 Hz, 3H), 1.93–1.03 (m, 2H), 2.03–2.08 (m, 1H), 2.34 (dddd, J = 9.7, 6.7, 4.4, 1.7 Hz, 1H), 3.50 (ddd, J = 12.0, 8.8, 3.4 Hz, 1H), 3.69 (dt, J = 12.0, 8.2 Hz, 1H), 4.25–4.22 (m, 2H), 5.29 (pd, J = 6.8, 1.9 Hz, 1H), 5.62–5.68 (m, 4H). 13C NMR (800 MHz, CD3OD, 25C): 18.61, 27.23 (6C), 23.12, 29.58, 39.74 (2C), 46.38, 60.12, 60.80, 75.87, 84.19, 84.31, 164.86, 171.65, 177.86, 177.91. HR-LCMS (ESI+): Calculated C21H35N2O10P + [M + H]+ = 507.21087; found [M + H]+ = 507. 20940, mass tolerance 0.1 mmu, retention time = 7.96 min.

Preparation of pCDP and inhibitor treatment solutions

All pCDPs were solubilized in DMSO to a stock concentration of 100 mM and stored at 4°C. The BACE1 inhibitor LY2811376 was solubilized in DMSO to a stock concentration of 10 mM and stored at –80°C. Further dilutions of these compounds were routinely prepared in DMSO (unless indicated

otherwise) and the final concentration of DMSO in media during all cell treatments or in all enzymatic assay solutions did not exceed 0.4%.

Cell treatments for analysis of AβPP processing

Cells were routinely plated and treated as described below unless otherwise indicated in the figure legends. Cells were plated at a density of 2×10^5 cells per well in six-well cluster dishes in 2 mL of complete media and grown for 16–24 h. Cells were washed twice with DMEM only and re-fed with 1 mL of complete media containing pCDPs, inhibitors or DMSO and incubated for 24 h. Cells were washed, re-treated for an additional 24 h and the conditioned media (CM) was collected and cleared by centrifugation at 12,000× g for 20 min at 4°C to remove intact cells and cellular debris. An aliquot of the cleared CM was combined with 4X Laemmli SDS-sample buffer containing 25 mM dithiothreitol (DTT) and used for the analysis of secreted AβPP fragments by immunoblotting. This same 48-h cell treatment procedure was performed to assess cell viability using a TC20 automated cell counter (BioRad), where live cells were distinguished by selective Trypan Blue staining of dead cells.

Preparation of cell lysates

Following the removal of the CM as described above, cell monolayers were washed twice with ice cold phosphate buffered saline (PBS) solution to remove residual media and lysed in 200–250 μL of lysis buffer (LB; 50 mM 4-(2-hydroxyethyl)-1-piperazineethanesulfonic acid (HEPES), pH 7.2, 150 mM NaCl, 2 mM Ethylenediaminetetraacetic acid (EDTA), 1% Triton X-100, 1 mM sodium orthovanadate, 50 mM sodium fluoride, 10 mM β-glycerophosphate, 500 μM 4-(2-Aminoethyl)benzenesulfonyl fluoride hydrochloride (AEBSF), 10 μg /mL Aprotinin, 10 μg/mL Leupeptin, and 5 μg/mL Pepstatin) for 30 min at 4°C with rocking. Crude lysates were collected and centrifuged at 28,000× g for 20 min at 4°C to remove cellular debris and insoluble material. The clarified whole cell lysates were removed, total protein was quantified using the DC Protein Assay with Bovine Serum Albumin (BSA) as a standard and then combined with 4X Laemmli SDS-sample buffer containing 25 mM DTT for analysis by immunoblotting.

Time course of pCDP-diBzl treatment

To obtain roughly the same protein levels and to harvest CM for all time points simultaneously, all cells were plated at the same time at a density of 2×10^5 cells per well in six-well cluster dishes in 2 mL of complete media and grown for 16–24 h. All wells were then washed twice with DMEM only and two wells were re-fed with 1 mL of complete media containing 400 μM of pCDP-diBzl, two wells were re-fed with 1 mL of complete media containing DMSO only, and the rest of the wells were re-fed with complete media only (48-h time point). After 24 h, media was removed from four currently untreated wells, washed with DMEM only, and then two wells were re-fed with 1 mL of complete media plus 400 μM of pCDP-diBzl while the other two wells were re-fed with 1 mL of complete media plus DMSO only (24-h time point). At approximately the same time, the cells for the 48-h time point were washed and re-fed with media containing DMSO or 400 μM of pCDP-diBzl for another 24 h (it was from this final 24-h collection period that the 48-h time point was collected). The same process was followed after an additional 12, 16, and 20 h to obtain the 12-, 8-, and 4-h treatment time points, respectively. At the end of the 48-h experiment, all CM was collected and cleared by centrifugation at 12,000× *g* for 20 min at 4°C to remove intact cells and cellular debris. An aliquot of the cleared CM was combined with 4X Laemmli SDS-sample buffer containing 25 mM DTT and used for the analysis of secreted AβPP fragments by immunoblotting. Cells were washed and lysed as described above.

Sodium dodecyl sulfate polyacrylamide gel electrophloresis (SDS-PAGE) and immunoblotting

Whole cell lysates (WCLs) and CM were prepared as described above and various amounts were analyzed by immunoblotting as indicated in the figure legends. Samples and protein standards were adjusted as needed to the desired total protein amount using LB (for WCL samples) or to equal volume using growth media (for CM samples). Housekeeping protein β–tubulin was used as a loading control for all WCL blots except those corresponding to treatments of H4-BACE1 cells, where Stain Free total protein provided a more reliable loading control at the high total protein loading level that was needed to detect endogenous AβPP [37].

All CM samples (except for sAβ, described below) were separated on 10% SDS-PAGE gels [38] and transferred to PVDF membrane without methanol [39] with constant cooling. Membranes were blocked with Tris-Buffered Saline with Tween (TBST; 25 mM Tris-HCl pH 7.2, 150 mM NaCl, and 0.1% Tween 20) containing 5% milk for 1-2 h at RT and then incubated with primary antibodies (diluted in TBST containing 0.5–1% BSA) at the following dilutions: anti-sAβPPα (EPR5119(2), 1:15,000) or anti-sAβPPβ (25 ng/mL). Anti-sAβPPα was incubated for 2-3 h at RT and anti-sAβPPβ antibody was incubated overnight at 4°C. Membranes were incubated for 2-3 h at RT with the appropriate HRP-conjugated secondary antibody (diluted 1:10,000 in TBST containing 1% milk). Pierce ECL Western Blotting substrate (for sAβPPα) or Pierce SuperSignal West Pico substrate (for sAβPPβ) were used to visualize the results on X-ray film. Band intensities were quantified by ImageJ and a background area of the same size was taken above each band and subtracted. These resulting values were first normalized to the averaged DMSO control for each protein and then further normalized for the total protein of the corresponding WCL for each sample (as determined by the DC Protein Assay).

All WCL samples were separated on 4–15% or 4–20% Mini Protean TGX Stain Free precast gels (Bio-Rad). Covalent coupling of the chromophore in the gel to the separated proteins was achieved using an activation time of 1 min. Proteins were transferred to Immun-Blot LF PVDF membrane with 10% methanol for 2 h at constant current of 250 mA [39]. Membranes were blocked with TBST containing 5% milk for 2 h at RT or overnight at 4°C. Each membrane was washed four times with TBST (5 min per wash). Membranes were incubated with anti-AβPP (Y188, 1:40,000) overnight at 4°C or for 2.5 h at RT, with anti-β–tubulin (1:30,000) for 2 h at RT, or with anti-BACE1 (1:5,000) for 4 h at RT. Membranes were incubated for 1.5–3 h at RT with the appropriate HRP-conjugated secondary antibody as described above.

For WCL blots of treated H4-BACE1 cells, proteins transferred membranes were first imaged using a stain free blot application on a Chemidoc MP system (Bio-Rad), then were incubated with Pierce SuperSignal West Pico Chemiluminescent Substrate for visualization. For all other WCL blots, Pierce SuperSignal West Pico Chemiluminescent Substrate (for comparison of AβPP levels across different cell models), Clarity Western ECL (for comparison of BACE1 levels across different cell models), or Pierce ECL Western Blotting Substrate (for AβPP and β-tubulin in H4-APP695 cells) were used for visualization. All blots were visualized using Chemi Hi Sensitivity blot application in the Chemidoc MP System (Bio-Rad). Band volumes were quantified using Image Lab (Bio-Rad). For use of β-tubulin as a loading control, desired protein band volumes in a given lane were normalized to the β-tubulin signal volume in that lane. For use of stain free total protein as a loading control, desired protein band volume(s) in each lane were normalized to total protein as quantified using Image Lab (Bio-Rad). For all WCL blots of FL-AβPP where mature and immature FL-AβPP were adequately resolved to allow quantification of each, previously normalized band volumes (for β-tubulin signal or stain free total protein) were further normalized to the average control immature AβPP band volume, as shown in the corresponding graphs.

Total secreted Aβ levels were determined by immunoblotting using the antigen epitope retrieval method essentially as described [40]. Briefly, 20 μL of conditioned media was separated in a 12.5% Bis-Tris-Mes gel and transferred to 0.2 μM nitrocellulose membranes for 90 min at 40 V using the BioRad Trans blotting system containing 20% methanol [39]. Membranes were steamed for 15 min to expose latent epitopes, blocked with TBST-milk and incubated with anti-Aβ antibody (1:4000) for 1 h at RT followed by overnight incubation at 4°C. Membranes were incubated with HRP-conjugated secondary antibody and results were visualized using the Pierce ECL Western Blotting substrate. Band intensities were quantified by ImageJ as described above.

Observation of pCDP uptake by LCMS

The following LCMS procedure for cell lysates was adapted from [41]. H4-AβPP695 cells were plated at a density of 1.5×10^6 cells per 10-cm dish (x20) in complete media and grown at 37°C in a humidified atmosphere (90%) containing 10% CO_2. After ~24 h, cells were re-fed with 5 mL of fresh media containing various pCDPs (400 μM) or DMSO as indicated in the figure legend (two plates per condition). The remaining ten plates were re-fed with 5 mL of fresh media and were used as a "spiked" positive control set. After 24 h, the treated cells were scraped into their conditioned media (duplicates were combined) and collected by centrifugation for 5 min at

2000× g at RT. The remaining 10 untreated dishes ("spiked" positive control set) were scraped, divided into five equal aliquots and cells were collected by centrifugation. Cell pellets were washed three times with cold (4°C) PBS to remove all residual conditioned media and pCDPs. Cell pellets were quick frozen in liquid nitrogen and stored at –80°C until lysis.

Frozen pellets were thawed on ice for 30 min, re-suspended in 500 μL of water and 500 μL of methanol, vortexed, and incubated on ice for 1 h to facilitate complete lysis. The five "spiked" positive control samples were prepared by adding 1 μL of 1 mM for each pCDP or DMSO (1:100 dilution of the stocks in water) to individual pellets, vortexed and incubated on ice for 1 h. Lysates were centrifuged at 15,000 RPM for 30 min at 4°C and the supernatants were collected and lyophilized to dryness. Each dried sample was dissolved in 300 μL of 1:1 methanol/water and 2 μL was separated using reverse-phase high resolution UHPLC-MS exactly as described above (see LCMS *Analysis* section of *Analysis of custom-synthesized compounds*). The Thermo-Scientific Xcalibur software package was used to visualize, analyze, and depict the LCMS data presented here.

BACE1 activity assay

BACE1 activity was determined by incubating 400 μM of individual pCDPs, the BACE1 inhibitor LY2811376 (positive control) or DMSO (negative control) in a reaction mixture containing 25 mM sodium acetate assay buffer, pH 4.42, 1% BSA, 0.2 μg of the catalytic domain of recombinant human BACE1 and 10 μM of Methyl cumaryl amide (Mca) fluorogenic substrate in a final volume of 110 μL. Fluorescence intensity was measured with a Synergy H1 hybrid reader (BioTek, Winooski, VT) (excitation 320 nm, emission 405 nm) using a black microplate with half-area wells and an opaque bottom with continuous gentle shaking at 37°C for 1 h with readings acquired every 5 min. Results were analyzed in Excel 2010 by averaging the DMSO control 1 h fluorescence intensity values and then normalizing all experimental results for pCDPs and BACE1 inhibitor to this value. The normalized data was then averaged over repeated points ($n = 6$ for all pCDP treatments and DMSO negative control, $n = 5$ for BACE1 inhibitor data), the standard deviations were determined, and the data were graphed using Excel 2010 software.

Statistical analysis

Averages, 20% Coefficient of Variation (CV), standard deviation (S.D.), and statistical analysis for significance via the unpaired, independent Student's T test for data were determined using Excel 2010. CM and WCL data were expressed as the mean ± 20% CV. CM data were deemed significant at $p < 0.05$. 20% CV was used as an estimate for western blot variability to yield more conservative assignments of statistical significance [37]. Cell viability data were expressed as mean ± S.D. and were deemed significant at $p < 0.05$. All graphs were generated in Excel 2010. Approximate EC50 values were determined by fitting the sAβPPβ level versus dose curves to the 4-parameter logistic model $Y = (d - a)/\{1 + (X/c)^b\}$, where a is the lower asymptote, d is the upper asymptote, X is the dose concentration, c is the concentration at which the sAβPPβ level is midway between a and d, and b is the slope factor that describes the steepness of the central linear portion of the curve [42]. Parameters a, b, c, and d were optimized by minimizing the sum of the squared differences between experimental and model-predicted values using the Solver add-in within Excel 2010 (Microsoft).

RESULTS

H4 neuroglioma cells stably overexpressing AβPP695 or BACE1 enable reliable detection of sAβPPβ

BACE1 cleavage of AβPP produces sAβPPβ and C99 fragments (Fig. 1A) and is essential for the production of Aβ. The C-terminal fragment, C99, is a transient intermediate in the amyloidogenic pathway that reflects the relative balance of multiple pathways. C99 is processed by γ-secretase [43], is also a substrate for α-secretase [44], and is turned over by both ERAD and ubiquitin-independent lysosomal degradation pathways [45]. Moreover, C99 can be additionally cleaved to C89 by BACE1 and BACE2 [46], and the proportion of C89 relative to C99 increases with increasing BACE1 expression [47]. In contrast, sAβPPβ (~100 kDa) is secreted to the medium and can be detected (and distinguished from sAβPPα) by antibodies specific for the C-terminus of sAβPPβ [48]. The sAβPPβ fragment therefore serves as an effective proxy for the maximum possible amyloidogenic processing; for every

Aβ peptide molecule produced, a corresponding sAβPPβ fragment must be generated. Importantly, sAβPPβ reflects the amount of AβPP that undergoes the entry step (i.e., β-secretase cleavage) into the amyloidogenic pathway (Fig. 1). Our goal was to generate two distinct cell lines, via overexpression of AβPP695 or BACE1 that recapitulate two distinct causative mechanisms of AD [16, 18, 49], to enable reliable detection of sAβPPβ for evaluating the effects of pCDP treatment on AβPP amyloidogenic processing.

The human H4 neuroglioma cell line, derived from a neuroglioma tumor and adapted for growth in culture [50, 51], has been broadly used in AD research [52–55]. In H4 cells, the endogenous AβPP751 isoform (Fig. 3A) predominantly undergoes non-amyloidogenic processing, as shown by the absence of sAβPPβ in 15 μL of CM (Fig. 3B) and the abundance of sAβPPα detected in just 2 μL of the same CM (Fig. 3C). To generate detectable levels of sAβPPβ, we chose to take two separate approaches: (1) increase the level of the AβPP695 isoform, since this is the predominant form found in neurons [56] and overexpression of AβPP695 is known to increase amyloidogenic processing [57], and (2) increase the level of BACE1 to shift the balance toward amyloidogenic processing [49].

To this end, we generated two distinct H4 cell lines that serve as AD models: the H4-AβPP695 cell line that overexpresses AβPP695 (wild-type) and the H4-BACE1 cell line that overexpresses BACE1 (wild-type) (Fig. 3A). The quantity of AβPP695 is increased approximately 15-fold in H4-AβPP695 lysates compared to endogenous AβPP751 in H4 and H4-BACE1 cell lysates, using β-tubulin for normalization across lanes (Fig. 3A). BACE1 is robustly detected in 6.8 μg of H4-BACE1 cell lysate, whereas endogenous BACE1 was not detected in 6.8 μg of H4 cell lysate (Fig. 3A). Additionally, the level of mature AβPP751 is reduced in the H4-BACE1 cells (Fig. 3A), which is consistent with previous results that have shown that most cleavage of AβPP via BACE1 happens after O-glycosylation [58].

As anticipated, both H4-AβPP695 and H4-BACE1 cell lines enable sensitive detection of sAβPPβ (Fig. 3B) and produce different relative levels of sAβPPα (Fig. 3C). With only 2 μL of CM, sAβPPα is detected in H4-AβPP695 cells after a 3-s exposure time (Fig. 3C, top blot). After a 2-min exposure of the same blot, the less abundant sAβPPα from both H4 and H4-BACE1 cells is detectable (Fig. 3C, bottom panel) at the expected (different) molecular weights. Due to robust overexpression of AβPP695 in the H4-AβPP695 cell line, the highly abundant sAβPPα secreted into CM (Fig. 3C) is not conducive to observing small changes in nonamyloidogenic processing. However, since AβPP expression remains at an endogenous level in the H4-BACE1 cell line, changes in both sAβPPβ (Fig. 3B) and sAβPPα (Fig. 3C) can be detected in CM, thereby allowing amyloidogenic and non-amyloidogenic processing of AβPP to be simultaneously monitored in this cell line. Collectively, these data demonstrate the utility of H4-AβPP695 and H4-BACE1 cells for monitoring sAβPPβ as a proxy for the amyloidogenic processing of AβPP.

The cis-locked pCDP mimic was derivatized to aid in cellular uptake

Since the *cis*-locked pCDP (Fig. 1C) is charged and is not expected to be taken up by cells, we prepared three derivatives that block the phosphate group and are more hydrophobic (Fig. 2). The phosphate group in pCDP (Fig. 2A) was protected by a single benzyl group (Fig. 2B), two benzyl groups (Fig. 2C), or two pivaloyloxymethyl (POM) groups (Fig. 2D). Notably, since the POM groups are easily removed by cellular esterases [59], the pCDP-diPOM molecule is a "pro-drug" version of the pCDP (Fig. 2A). All pCDPs were analyzed by ^{1}H NMR and LCMS to verify their structure and MW (Supplementary Figures 1–5).

Only pCDP-diBzl reduces sAβPPβ in the conditioned media of H4-AβPP695 cells

Using sAβPPβ as a proxy for monitoring amyloidogenic processing of AβPP, the effects of the pCDP compounds (Fig. 2) were investigated in H4-AβPP695 cells. H4-AβPP695 cells were treated with 400 μM of pCDP, pCDP-Bzl, pCDP-diBzl, and pCDP-diPOM for a total of 48 h and 15 μL of CM from the final 24 h of treatment was analyzed by western blot for changes in sAβPPβ (Fig. 4A). Only pCDP-diBzl had a potent effect on the quantity of sAβPPβ present in the media, severely reducing the amount of detectable sAβPPβ to less than 1% of the control without a notable change in the levels of mature or immature FL-AβPP (Fig. 4A). The well-characterized BACE1 inhibitor (LY2811376) was also used to treat cells at 2.5 μM (Fig. 4A) and exhibited a similar effect on H4-AβPP695 cell line as the pCDP-diBzl. The other CDP variants (pCDP, pCDP-Bzl, pCDP-diPOM) had little to no effect on

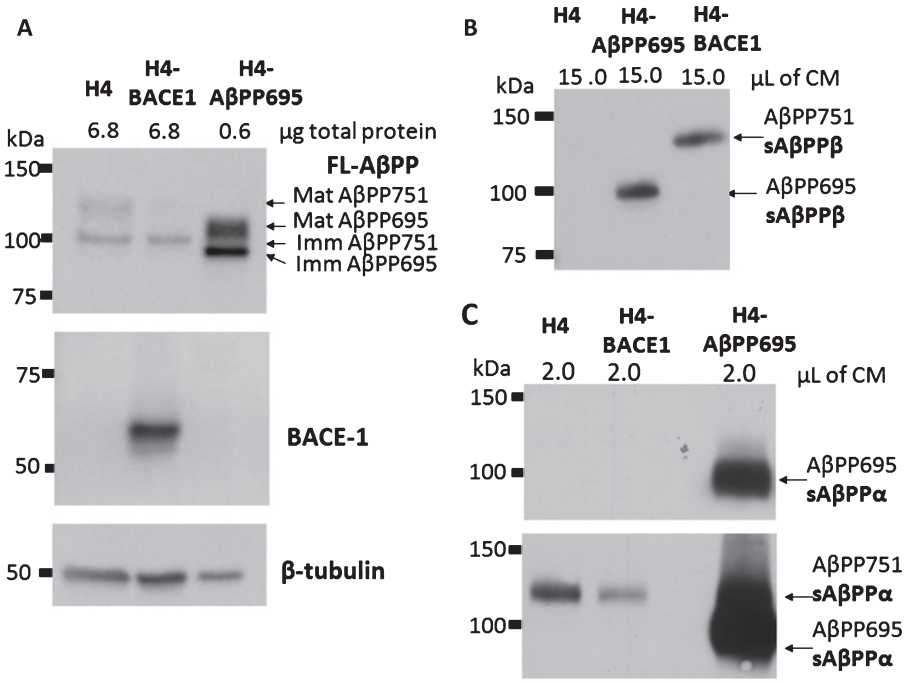

Fig. 3. H4 neuroglioma cell lines transfected with AβPP695wt (H4-AβPP695) or BACE1 (H4-BACE1) show increased production of AβPP proteolytic products. Western blot analysis of full-length AβPP in cell lysates (A), and of sAβPPβ and sAβPPα in conditioned media (B,C). MW differences reflect exogenous AβPP695 in H4-AβPP695 versus endogenous AβPP751 in H4 and H4-BACE1. A) Full-length AβPP (top panel), BACE1 (middle panel) and β-tubulin (bottom panel) in WCL from H4, H4-BACE1 and H4-AβPP695 cells (total protein loaded: 6.8 µg, 6.8 µg and 0.6 µg, respectively). B) sAβPPβ in 15 µL CM from H4, H4-AβPP695, and H4-BACE1 cells. C) sAβPPα in 2 µL CM from H4, H4-BACE1, and H4-AβPP695 cells (top: 3-s exposure time; bottom: 2-min exposure time).

the amount of sAβPPβ, despite their related structure. To assess the impact of pCDP-diBzl treatment on cell viability, H4-AβPP695 cells were treated with 200 µM and 400 µM of pCDP-diBzl for 48 h, trypsinized, stained with Trypan Blue, and counted. Although growth seemed to be slowed in the presence of 200 µM and 400 µM pCDP-diBzl, no significant toxicity was observed (>96% of all cells counted were alive) (Supplementary Figure 6).

A dose-dependence experiment using 25, 50, 100, 200, and 400 µM of pCDP-diBzl was performed to monitor changes in sAβPPβ in H4-AβPP695 cells (Fig. 4B). As shown, 48 h of treatment with 400 µM of pCDP-diBzl has the most potent impact on sAβPPβ levels (Fig. 4B) with an approximate EC50 value of 126 µM (Fig. 4B). As described above, the robust production of sAβPPα in these cells (Fig. 3C) prevents reliable evaluation of small changes in the non-amyloidogenic pathway. The mature and immature AβPP signal for the DMSO and 400 µM pCDP-diBzl samples from Fig. 4A and B were combined ($n = 4$) and, for this highest level of treatment with pCDP-diBzl, no significant impact on full length AβPP (FL-AβPP) levels was observed (Fig. 4C). A same dose-dependent response was also observed on sAβ levels in H4-AβPP695 cells (Fig. 4D) with no significant impact on FL-AβPP signal. Additionally, a time-dependence study was performed to see if 48 h of treatment was crucial for the observed effect on sAβPPβ reduction (Fig. 4E). A short exposure time (30 s) shows clear reduction of sAβPPβ in CM of pCDP-diBzl treated cells for 12, 24, and 48 h total time periods (Fig. 4E, left). A much longer exposure (10 min) reveals additional observable reduction of sAβPPβ at 4 h (Fig. 4E, right), whereas sAβPPβ was not yet detectable even in untreated cells at 2 h (data not shown). These data demonstrate that pCDP-diBzl treatment of H4-AβPP695 cells reduces secreted sAβPPβ levels without significantly changing FL-AβPP levels, and that this reduction is evident at the earliest time point at which sAβPPβ can be detected.

pCDP-diBzl and pCDP-diPOM reduce sAβPPβ in the conditioned media of H4-BACE1 cells

As was observed in the H4-AβPP695 cells, treatment of H4-BACE1 cells with 400 µM of

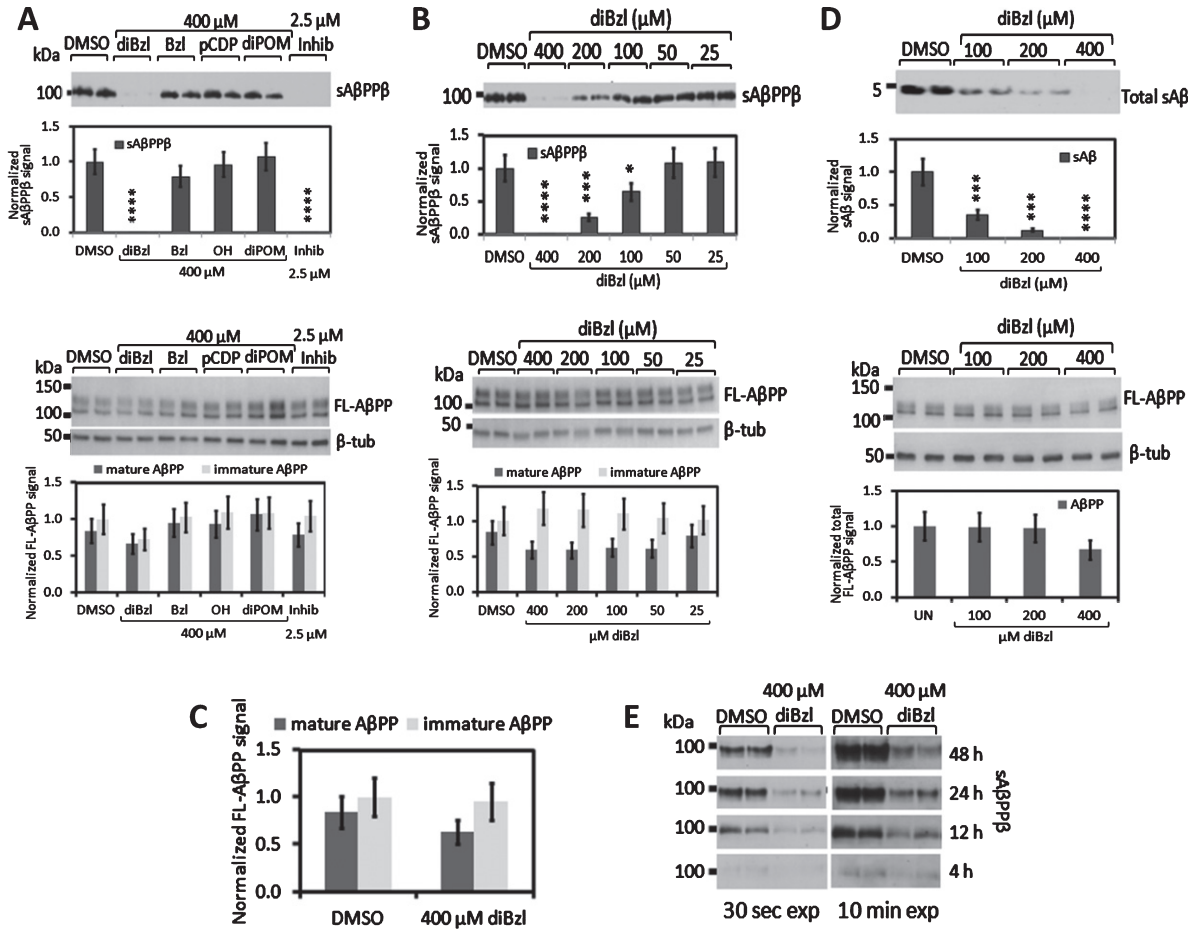

Fig. 4. pCDP-diBzl reduces sAβPPβ levels in dose- and time-dependent manners in H4-AβPP695 cells. Western blot analysis in H4-AβPP695 cells of sAβPPβ levels (A, B, and E) resulting from treatment with different pCDP compounds (A), treatment with different doses of pCDP-diBzl (B), and time-dependence of pCDP-diBzl treatment (E), and of sAβ levels resulting from treatment with different doses of pCDP-diBzl (D). A) sAβPPβ in 15 µL CM (top panel) and full-length AβPP in 0.6 µg total WCL protein (bottom panel) resulting from duplicate treatments with 400 µM of pCDP-diBzl (diBzl), pCDP-Bzl (Bzl), pCDP, and pCDP-diPOM (diPOM), with 2.5 µM of BACE1 inhibitor LY2811376 (Inhib) and DMSO (control) for 48 h total. Quantified levels of sAβPPβ (Mean ± 20% CV, $n = 4$, each) were statistically analyzed by the Student's T test (*$p < 0.05$; **$p < 0.01$; ***$p < 0.001$; ****$p < 0.0001$). Quantified levels of full length AβPP (mature and immature) were normalized to β-tubulin (Mean ± 20% CV, $n = 2$, each). B) As in A, resulting from dose-dependence of pCDP-diBzl treatment. Duplicate treatments were performed with 25, 50, 100, 200, and 400 µM of pCDP-diBzl and DMSO (control) for 48 h total. Data were quantified and statistically analyzed as in A. C) DMSO and 400 µM diBzl data points for mature-AβPP and immature-AβPP (from A and B) were combined ($n = 4$, each) and statistically analyzed as in A. D) sAβ in 20 µL CM (top panel) and full-length AβPP in 1 µg total WCL protein (bottom panel) resulting from treatment with 100, 200, and 400 µM of pCDP-diBzl for 48 h total. Data were quantified and statistically analyzed as in A. E) sAβPPβ in 15 µL CM resulting from treatment with pCDP-diBzl (400 µM) for 4, 12, 24, and 48 consecutive h (left panels: 30-s exposure time; right panels: 10-min exposure time).

pCDP-diBzl yielded a similar decrease in sAβPPβ without a significant impact on FL-AβPP levels (Fig. 5A). Additionally, sAβPPα (derived from endogenous AβPP751 in these cells) does not significantly change upon treatment with any of the pCDP compounds, and shows no significant dose-dependence with pCDP-diBzl treatment (Fig. 5). The dose-dependent reduction of sAβPPβ induced by pCDP-diBzl treatment of H4-BACE1 cells (Fig. 5B) is similar to what was observed in H4-AβPP695 cells, with an EC50 value of approximately 67 µM (Fig. 5B). Again, mature and immature FL-AβPP signal for the DMSO and 400 µM pCDP-diBzl samples from Fig. 5A and B were combined ($n = 4$) to show no significant impact on FL-AβPP levels (Fig. 5C). The similar dose dependence and EC50 values in these distinct cell lines, where either AβPP or BACE1 are significantly overexpressed, indicate

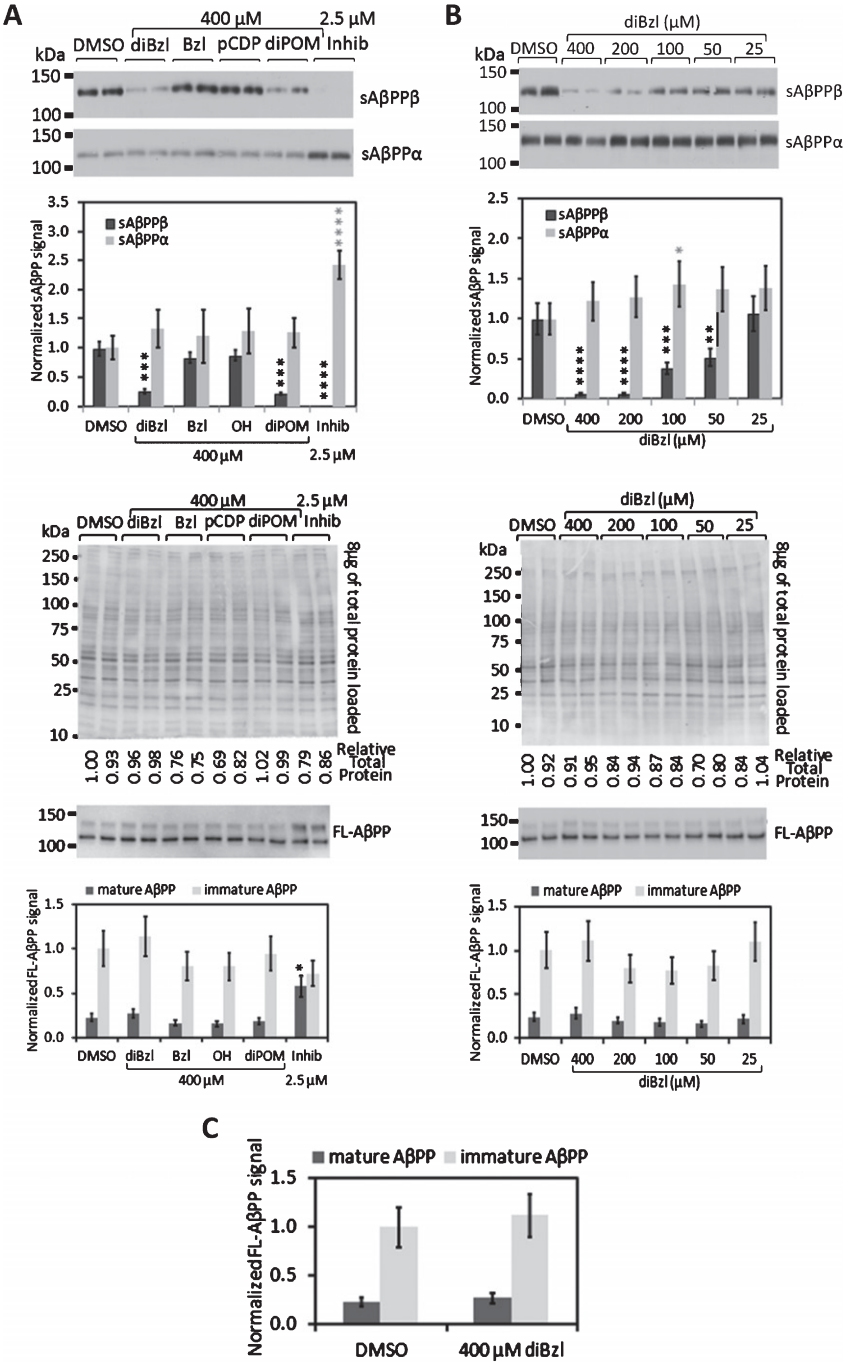

Fig. 5. pCDP-diBzl reduces sAβPPβ levels in a dose-dependent manner in H4-BACE1 cells. Western blot analysis of sAβPPβ and sAβPPα levels in H4-BACE1 cells resulting from treatment with different pCDP compounds (A) and with different doses of pCDP-diBzl (B). A) sAβPPβ and sAβPPα in 15 µL CM (top panels), and full-length AβPP in 8 µg total WCL protein with corresponding stain free total protein image (bottom panels) resulting from duplicate treatments with 400 µM of pCDP-diBzl (Bzl), pCDP-Bzl (Bzl), pCDP, and pCDP-diPOM (diPOM), with 2.5 µM of BACE1 inhibitor LY2811376 (Inhib), and DMSO (control) for 48 h total. Quantified sAβPPα and sAβPPβ (Mean ± 20% CV, $n = 4$, each) were statistically analyzed by the Student's T test ($^{*}p < 0.05$; $^{**}p < 0.01$; $^{***}p < 0.001$; $^{****}p < 0.0001$). Quantified levels of full length AβPP (mature and immature) were normalized to stain free total protein (Mean ± 20% CV, $n = 2$, each). B) As in A, resulting from dose-dependence of pCDP-diBzl treatment. Duplicate treatments were performed with 25, 50, 100, 200, and 400 µM of pCDP-diBzl and DMSO (control) for 48 h total. Data were quantified and statistically analyzed as in A. C) DMSO and 400 µM diBzl data points for mature-AβPP and immature-AβPP (from A and B) were combined ($n = 4$, each) and statistically analyzed as in A.

that pCDP-diBzl does not act through direct competition for a binding partner of either AβPP or BACE1. These data further suggest that pCDP-diBzl might act in both distinct cell lines via a common mechanism to reduce sAβPPβ. In contrast, while 400 μM pCDP-diPOM treatment of H4-AβPP695 cells showed no significant effect, treatment of H4-BACE1 cells with 400 μM pCDP-diPOM significantly reduced the amount of sAβPPβ without changing FL-AβPP signal (Fig. 5A, B). Although this 5-fold reduction is approximately the same as the effect of pCDP-diBzl treatment in these cells, the observation that pCDP-diPOM is ineffective in cells overexpressing AβPP is consistent with a mechanism of action in which pCDP-diPOM blocks AβPP interaction with an amyloidogenic binding partner.

As expected, treatment with 2.5 μM BACE1 inhibitor LY2811376 again inhibits sAβPPβ production in H4-BACE1 cells. Interestingly, a clear, significant increase in both sAβPPα and mature (glycosylated) full length AβPP is observed in this cell model, where only endogenous AβPP751 is expressed (Fig. 5A). This suggests that direct inhibition of BACE1 catalytic cleavage of AβPP might increase recycling of AβPP back to the plasma membrane via trafficking of endocytosed AβPP back to the trans-Golgi network and subsequent secretory pathway, where glycosylation and β-secretase activities are active. This effect is not observed in treatments with 400 μM pCDP-diBzl or 400 μM pCDP-diPOM and suggests a different mechanism for these molecules.

Association of pCDPs with and their conversion by H4-AβPP695 cells

To gain insight regarding the fate of pCDPs inside cells, LCMS was used to detect the presence of each compound in lysates from H4-AβPP695 cells treated with the various pCDPs. Importantly, these lysates were extracted using 1:1 methanol/water by volume, which is expected to at least partially solubilize most polar lipids and to denature some proteins. Although the pCDP variants are chemically very similar, LCMS was highly effective for detecting the pCDP variant and its conversion products. The neutral-charge MW of each pCDP molecule is shown in Fig. 2 and the electrospray ionization in positive mode (ESI+) MW for each pCDP is the following: 279 for pCDP, 369 for pCDP-Bzl, 459 for pCDP-diBzl, and 507 for pCDP-diPOM.

For comparison, lysates from cells treated with 400 μM of each pCDP variant (Fig. 6A) and lysates from untreated cells that were spiked with 100 μM of respective pCDPs (Fig. 6B) were analyzed by LCMS. Lysate from cells treated with 400 μM of pCDP-diBzl displays not only the expected MW 459 but also a substantial amount of MW 369, corresponding to pCDP-Bzl. In contrast, lysate from untreated cells spiked with pCDP-diBzl shows predominantly MW 459 and significantly lower MW 369. This suggests that pCDP-diBzl is converted to pCDP-Bzl inside the cell. Similarly, treatment with 400 μM of pCDP-diPOM shows an elevated amount of MW 279 and no detectable MW 507, while the untreated cell lysate spiked with pCDP-diPOM shows a substantial peak only for MW 507 (Fig. 6). This supports successful entry of pCDP-diPOM into cells where active esterases efficiently cleave the POM groups *in vivo* [59], whereas esterase activity in the spiked case could be inhibited in 1:1 methanol/water. Lysate from pCDP-Bzl treated cells does show MW 369, demonstrating that the pCDP-Bzl molecule does associate with cells, although as shown above it does not significantly reduce sAβPPβ (Fig. 4A). Cells treated with pCDP do not show MW 279 significantly above the DMSO control, but spiked cells with pCDP do, indicating that although pCDP itself is detectable it does not associate with treated cells sufficiently enough to be detected. Together, these results show that pCDP-diBzl, pCDP-Bzl, and pCDP-diPOM associate with H4-AβPP695 cells, and that pCDP-diBzl and pCDP-diPOM are modified by the cell.

pCDPs do not specifically inhibit the catalytic activity of BACE1

Since a reproducible effect on reduction of sAβPPβ by pCDP-diBzl and pCDP-diPOM was observed, we sought to determine whether these compounds directly inhibit the activity of the BACE1 catalytic domain. Using recombinant human BACE1 catalytic domain and an intra-molecularly quenched Mca fluorogenic substrate as part of a FRET-based assay [60], we tested 400 μM of each pCDP variant for inhibition of BACE1catalytic activity. Additionally, we tested the known BACE1 inhibitor LY2811376 at 2.5 μM as a positive control for reduced BACE1 catalytic activity. As shown in Fig. 7, while LY2811376 showed a potent decrease as expected, we saw no significant decrease in the catalytic activity of recombinant, purified BACE1

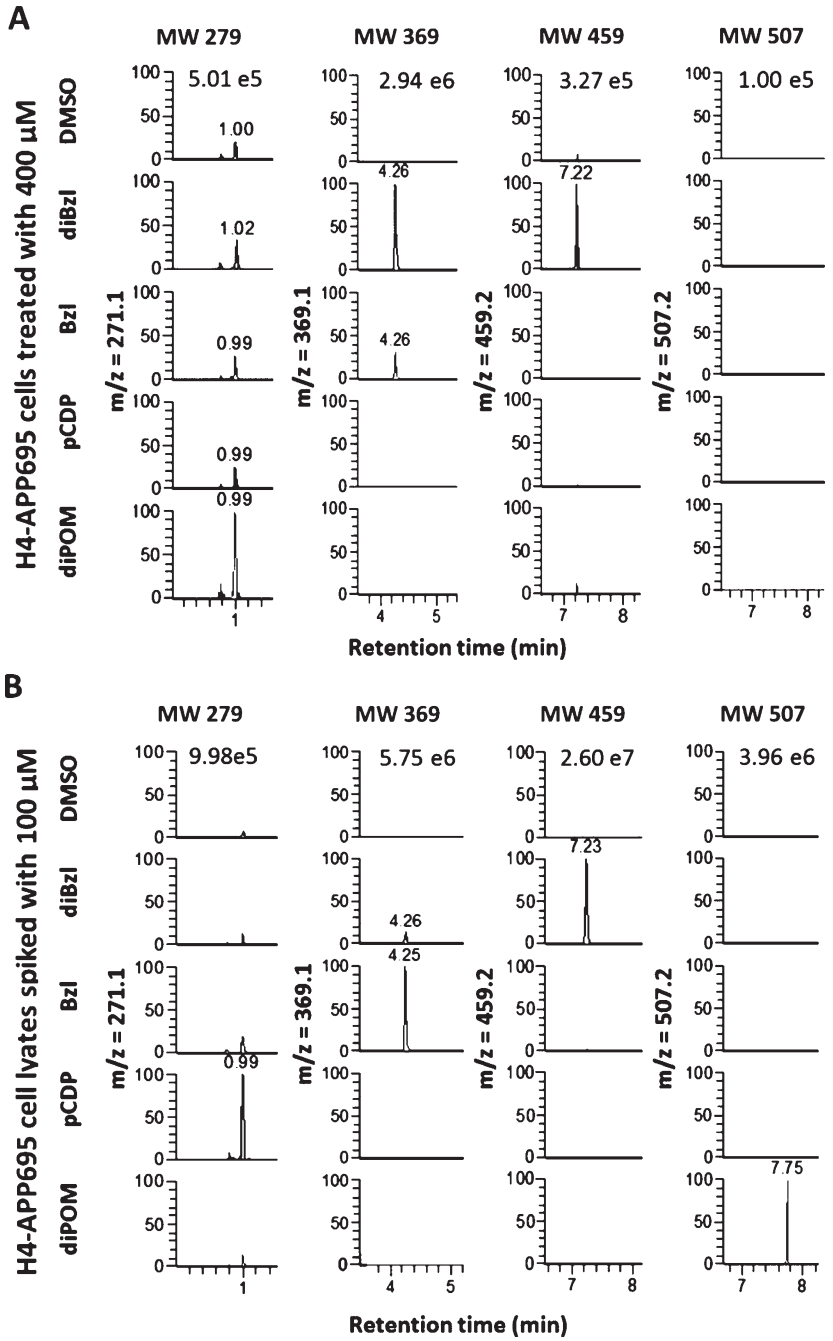

Fig. 6. ESI+ LCMS results show selective uptake and conversion of pCDPs. H4-AβPP695 cells were treated with 400 μM of DMSO (control), pCDP- diBzl (diBzl), pCDP-Bzl (Bzl), pCDP, and pCDP-diPOM (diPOM) for 24 h and lysates are analyzed by ESI+ LCMS (A). Untreated H4-AβPP695 cells were also lysed and spiked with 100 μM DMSO, diBzl, Bzl, pCDP, and diPOM to act as positive controls (B). Total Ion Chromatograms (TICs) for treated and positive controls were analyzed to find MWs 279 (279.07360, mass tolerance 0.1 mmu), 369 (369.12050, mass tolerance 0.5 mmu), 459 (459.16706, mass tolerance 0.1 mmu), and 507 (507.20940, mass tolerance 0.1 mmu) (A, B). All of the graphs (A, B) show relative abundance of these specific MWs and peaks are labeled with retention time.

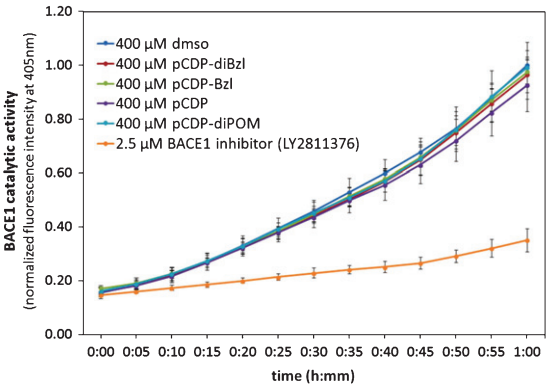

Fig. 7. pCDPs do not specifically inhibit the catalytic activity of BACE1. The activity of the BACE1 catalytic domain is observed through the cleavage of the Mca fluorogenic substrate. For each time point, the average is plotted ($n=6$, and $n=5$ for BACE1 inhibitor data) and error (±S.D.) was determined. Intensity is normalized to the 1-h fluorescence intensity for the DMSO control sample.

catalytic domain with any of pCDP variants at 400 µM (as measured by fluorescence intensity). These results demonstrate that pCDP-diBzl and pCDP-diPOM do not act as a direct inhibitor of BACE1 catalytic activity, and point to an alternate mechanism by which they inhibit amyloidogenic AβPP processing in H4 cell models of AD.

DISCUSSION

The effective treatment of AD will require an in-depth understanding of key interactions that mediate the amyloidogenic processing of AβPP. Although BACE1 cleavage of AβPP initiates this process, therapeutic strategies to inhibit this catalytic reaction are complicated by the essential functions of BACE1 that include myelination, axon guidance, muscle spindle formation, and neuronal network functions (reviewed in [61]). Hence, an agent that could specifically reduce BACE1 cleavage of AβPP without reducing its cleavage of other normal cellular targets is highly desirable. In this study, we have investigated the possibility that the *cis* conformation of a phospho-Thr-Pro peptide bond in the cytoplasmic tail of AβPP might function as a signal for increased amyloidogenic AβPP processing. We designed and synthesized four "*cis*-locked" pCDP compounds and tested their effect on sAβPPβ production in two distinct AD cell models. Using this approach, we have demonstrated that one specific pCDP derivative, pCDP-diBzl, is active in suppressing amyloidogenic processing of AβPP in both H4-AβPP695 and H4-BACE1 cell models. Additionally, a second derivative, pCDP-diPOM, has a similar effect but only in H4-BACE1 cells, where solely endogenous AβPP is expressed. Moreover, we have demonstrated that neither the pCDP-diBzl nor the pCDP-diPOM directly inhibits the BACE1 catalytic site *in vitro*. These findings support a pathogenic role of the *cis* conformation in promoting amyloidogenic AβPP processing, and open new avenues toward the development of AβPP-specific therapeutic agents to inhibit this role.

An important consideration to address is what the active form of each compound is in the cell. Our LCMS data of lysates from cells treated with pCDP-diPOM shows full deprotection of pCDP-diPOM to pCDP, which allows us to conclude that the effective form of pCDP-diPOM in treated cells is the deprotected pCDP. Of the molecules tested, pCDP is the closest mimic of phosphoThr-Pro, thus it is expected to be less effective in a background of excess AβPP (as in H4-AβPP695 cells), providing a plausible explanation for why it does not work in H4-AβPP695 cells. For the pCDP-diBzl compound, our LCMS data of lysates from cells treated with this compound shows that pCDP-diBzl is partially converted to pCDP-Bzl. Importantly, direct treatment with pCDP-Bzl did not display significant activity in either cell type, even though it is observed in lysates from H4-AβPP695 cells. Thus, the active form in pCDP-diBzl treated cells is most likely pCDP-diBzl, although the prominent level of pCDP-Bzl in these cells cannot be ruled out as possibly contributing to activity.

We have employed two distinct cell models to investigate what are potentially multi-target mechanisms of these compounds. Our H4-AβPP695 and H4-BACE1 cell lines provide comparative disease models in which two distinctly different perturbations, the overexpression of AβPP or BACE1, both recapitulate the disease state as measured by elevated amyloidogenic AβPP processing. Since AD is a complex disease with many potential targets that can influence AβPP processing [62], and given the known pleiotropic effects of diketopiperizine molecules [3], it is plausible that the observed effects of these compounds involve multiple targets. Indeed, the use of both AD cell models reveals that pCDP-diBzl and pCDP-diPOM have at least partially different mechanisms of activity. The observation that pCDP-diBzl has a similar dose-dependence in both models suggests that its primary target is not a direct

binding partner of either AβPP or BACE1, which are each robustly overexpressed in their respective cell lines. This would potentially rule out numerous cellular factors as pCDP-diBzl targets known to directly bind to AβPP [63]. However, the inability of pCDP-diPOM to alter amyloidogenic processing of AβPP in H4-AβPP695 cells suggests that the target of pCDP-diPOM may indeed be an amyloidogenic-promoting binding partner of AβPP, whereby the robust over expression of AβPP in H4-AβPP695 cells prevents effective inhibition of this pathogenic interaction. Moreover, the effectiveness of pCDP-diPOM in H4-BACE1 cells, where BACE1 is robustly overexpressed, supports the possibility that pCDP-diPOM blocks an AβPP-specific binding partner.

The pattern of AβPP proteolytic products induced by compound treatments offers clues regarding potential mechanisms of pCDP-diBzl and pCDP-diPOM activities. Specifically, both compounds reduced sAβPPβ and total secreted Aβ levels without significantly changing sAβPPα or mature AβPP (mat AβPP) levels. These observations suggest that these compounds do not significantly increase levels of AβPP at the plasma membrane (which should increase sAβPPα), and do not increase AβPP levels in the ER/Golgi secretory pathway (which should increase matAβPP). The observation of this same pattern of AβPP proteolytic products with both compounds suggests that pCDP-diPOM and pCDP-diBzl might act at a common point in the complex system of networks that govern AβPP processing. BACE1 cleavage of AβPP, which produces sAβPPβ and is the first requisite step in the production of Aβ, involves additional regulatory factors that could serve as targets of pCDP-diBzl and pCDP-diPOM. While BACE1 endocytosis is ARF6-dependent [64], AβPP is internalized via clathrin-dependent endocytosis (reviewed in [63]). The sorting of AβPP and BACE1 into common intracellular acidic vesicles via different pathways [65], which is central to BACE1 cleavage of AβPP [66–68], offers many potential targets [63]. Together, these results suggest a model in which both pCDP-diBzl and pCDP-diPOM inhibit the association of AβPP and BACE1 and subsequent generation of sAβPPβ, but that their activities are mediated through different targets (Fig. 8).

While additional studies are underway to elucidate the specific mechanisms by which pCDP-diBzl and pCDP-diPOM inhibit amyloidogenic processing, it is informative to consider mechanisms deduced for other small molecules that alter AβPP proteolytic processing. For example, treatment of rat primary cortical neurons with statins similarly decreases secreted Aβ, but significantly reduces matAβPP via a cholesterol-independent mechanism that involves selective reduction of AβPP phosphorylation at Thr668 [69], pointing to a central role of Thr668 phosphorylation in AβPP processing. In another example, treatment of HEK293 cells with the natural product 2,2',4'-trihydroxychalcone from *Glycyrrhiza glabra* (liquorice) root, reduced sAβPPβ without significant change in matAβPP (as we observe here), by serving as a non-competitive inhibitor of BACE1 catalytic activity [70]. Finally, the metal chelator clioquinol and various derivatives potently inhibit Aβ accumulation in cell models and in mice [71–75]. Treatment of AβPP-CHO cells with clioquinol alone reduced total sAβPP (sAβPPα and sAβPPβ were not distinguished), but the robust reduction of secreted $A\beta_{40}$ by clioquinol required co-treatment with copper (Cu^{2+}) [75]. The deduced mechanism was via activation of PI3K-Akt and JNK signaling pathways, culminating in the upregulation of secreted matrix metalloproteases (MMPs) that degrade extracellular Aβ [75]. However, the mechanism by which total sAβPP was reduced was not elucidated.

Interestingly, there is an additional mechanism by which clioquinol upregulates MMPs and Aβ clearance, with a possible link to AβPP proteolytic processing. Quinol family compounds, including clioquinol, inhibit the hydroxylation activity of Factor Inhibiting HIF-1 (FIH-1), one of the two distinct enzymes that initiate unbiquitin-mediated proteasomal degradation of hypoxia-inducible factor-1α (HIF-1α) [76–79]. Under low oxygen levels where FIH-1 activity is low, the stabilized HIF-1α induces expression of numerous genes, including MMPs [80, 81]. Hence, the inhibition of FIH-1 by clioquinol stabilizes HIF-1α, which leads to the upregulation of MMPs and subsequent rapid degradation of extracellular Aβ. HIF-1α is stabilized by direct interaction with COPS5 (also known as Jab1), a protein implicated in amyloidogenic processing of AβPP [75, 82]. Thus, an additional impact of clioquinol might be to induce elevated HIF-1α levels that compete for COPS5 binding to and stabilization of an amyloidogenic factor, thereby indirectly reducing amyloidogenic processing of AβPP. The multiple signaling pathways that respond to clioquinol, and the COPS5-mediated link between HIF-1α and amyloidogenic AβPP processing, exemplify the many interconnected systems of networks that govern the proteolytic fate of AβPP.

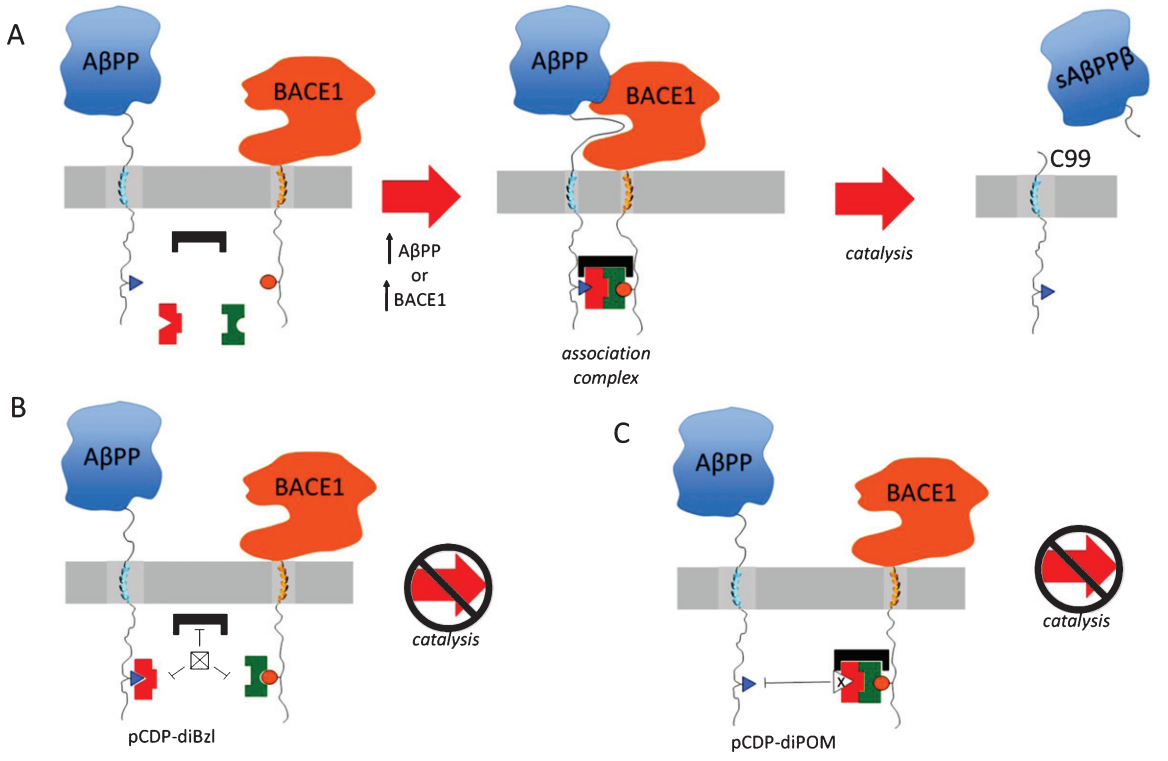

Fig. 8. Proposed model for pCDP-diBzl and pCDP-diPOM mechanisms of action. A) The disease state, induced by elevated expression of either AβPP695 or BACE1, increases the association of AβPP and BACE1 via a cytoplasmic association complex that promotes sAβPPβ production. B) pCDP-diBzl is proposed to inhibit formation of the association complex, independent of AβPP and BACE1 binding surfaces. C) pCDP-diPOM is proposed to inhibit formation of the association complex by directly blocking the AβPP binding partner in the association complex.

In conclusion, AD is a multifactorial disease that involves factors at the genetic, epigenetic, interactome, and environmental levels [62]. To understand such a multi-scale complex system, eukaryotic cell models that simulate the disease state are of great value. Here, we have used two distinct H4 neuroglioma cell lines, each with elevated expression of a single component involved in AβPP processing, to test compounds that mimic the *cis* conformation of a phospho-Thr-Pro peptide bond in the cytoplasmic tail of AβPP. The activity of pCDP, when delivered to the cell as its precursor pCDP-diPOM, suggests that the *cis* conformation of the phospho-Thr668-Pro669 motif in AβPP serves as a signal that increases association of AβPP and BACE1, since pCDP is the closest mimic of phosphoThr-Pro and is only active when endogenous levels of AβPP are present. Conversely, the similar activity of pCDP-diBzl in both comparative AD cell models points to a different target for this compound and suggests that the *cis* conformation is a broadly used signal, consistent with the wide array of diketopiperizine bioactivities [3]. Based on these results, we propose a model in which our two identified active compounds act through different targets, but at comparable points in AβPP processing system (Fig. 8). This model provides a framework for investigation of pCDPs binding to specific components of putative association complexes, and for further development of compounds that effectively block interactions that promote Aβ production. Overall, our studies support the idea that the *cis* isomer is a pathogenic conformation in the determination of AβPP proteolytic fate, and show that small molecules that mimic this conformation reduce amyloidogenic processing of AβPP. These findings provide important insights for guiding the future development of novel AD therapeutics.

ACKNOWLEDGMENTS

The authors thank Volker Vogt and Bill Brown for careful reading of the manuscript; the Craighead Lab for use of their microplate reader and Sarah

Reinholdt for technical assistance; Alex Artyukhin and Joshua Baccile for assistance with the UPLC-HRMS system, data acquisition, and analysis; Holger Sondermman for the generous use of western blot reagents and expertise; Carolyn Sevier for the use of the Chemidoc MP System in her laboratory; Susan E. Coombs for the generous contribution of the TC20 machine and slides for the viability assay; David Shalloway for use of lab and tissue culture room; David Kiemle for running NMR experiments on the Bruker Avance 800 MHz NMR with cryo probe at SUNY-ESF (funded by NIH shared instrumentation grant 1S10OD012254). This work was supported by NIH grant 1R21AG042056 (L.K.N.), NSF grant MCB-1157806 (L.K.N.) and NSF Graduate Research Fellowship (C.L.F.).

Authors' disclosures available online (http://j-alz.com/manuscript-disclosures/16-0051r2).

SUPPLEMENTARY MATERIAL

The supplementary material is available in the electronic version of this article: http://dx.doi.org/10.3233/JAD-160051.

REFERENCES

[1] Arunrattiyakorn P, Nitoda T, Kanzaki H (2006) Enzymatic conversion-based method for screening cyclic dipeptide-producing microbes. *Peptides* **27**, 633-639.

[2] Borthwick AD (2012) 2,5-Diketopiperazines: Synthesis, reactions, medicinal chemistry, and bioactive natural products. *Chem Rev* **112**, 3641-3716.

[3] Cornacchia C, Cacciatore I, Baldassarre L, Mollica A, Feliciani F, Pinnen F (2012) 2,5-diketopiperazines as neuroprotective agents. *Mini Rev Med Chem* **12**, 2-12.

[4] Prasad C (1995) Bioactive cyclic dipeptides. *Peptides* **16**, 151-164.

[5] Goolcharran C, Borchardt RT (1998) Kinetics of diketopiperazine formation using model peptides. *J Pharm Sci* **87**, 283-288.

[6] Prasad C, Peterkofsky A (1976) Demonstration of pyroglutamylpeptidase and amidase activities toward thyrotropin-releasing hormone in hamster hypothalamus extracts. *J Biol Chem* **251**, 3229-3234.

[7] Liu J, Brahimi F, Saragovi HU, Burgess K (2010) Bivalent diketopiperazine-based tropomysin receptor kinase C (TrkC) antagonists. *J Med Chem* **53**, 5044-5048.

[8] Houston DR, Synstad B, Eijsink VG, Stark MJ, Eggleston IM, van Aalten DM (2004) Structure-based exploration of cyclic dipeptide chitinase inhibitors. *J Med Chem* **47**, 5713-5720.

[9] Brauns SC, Milne P, Naude R, Van de Venter M (2004) Selected cyclic dipeptides inhibit cancer cell growth and induce apoptosis in HT-29 colon cancer cells. *Anticancer Res* **24**, 1713-1719.

[10] Faden AI, Knoblach SM, Cernak I, Fan L, Vink R, Araldi GL, Fricke ST, Roth BL, Kozikowski AP (2003) Novel diketopiperazine enhances motor and cognitive recovery after traumatic brain injury in rats and shows neuroprotection *in vitro* and *in vivo*. *J Cereb Blood Flow Metab* **23**, 342-354.

[11] Selkoe DJ (1994) Cell biology of the amyloid beta-protein precursor and the mechanism of Alzheimer's disease. *Annu Rev Cell Biol* **10**, 373-403.

[12] Kang J, Lemaire HG, Unterbeck A, Salbaum JM, Masters CL, Grzeschik KH, Multhaup G, Beyreuther K, Muller-Hill B (1987) The precursor of Alzheimer's disease amyloid A4 protein resembles a cell-surface receptor. *Nature* **325**, 733-736.

[13] Zhang H, Ma Q, Zhang YW, Xu H (2012) Proteolytic processing of Alzheimer's beta-amyloid precursor protein. *J Neurochem* **120**(Suppl 1), 9-21.

[14] Esch FS, Keim PS, Beattie EC, Blacher RW, Culwell AR, Oltersdorf T, McClure D, Ward PJ (1990) Cleavage of amyloid beta peptide during constitutive processing of its precursor. *Science* **248**, 1122-1124.

[15] Sinha S, Anderson JP, Barbour R, Basi GS, Caccavello R, Davis D, Doan M, Dovey HF, Frigon N, Hong J, Jacobson-Croak K, Jewett N, Keim P, Knops J, Lieberburg I, Power M, Tan H, Tatsuno G, Tung J, Schenk D, Seubert P, Suomensaari SM, Wang S, Walker D, Zhao J, McConlogue L, John V (1999) Purification and cloning of amyloid precursor protein beta-secretase from human brain. *Nature* **402**, 537-540.

[16] Holsinger RM, McLean CA, Beyreuther K, Masters CL, Evin G (2002) Increased expression of the amyloid precursor beta-secretase in Alzheimer's disease. *Ann Neurol* **51**, 783-786.

[17] Cataldo AM, Petanceska S, Peterhoff CM, Terio NB, Epstein CJ, Villar A, Carlson EJ, Staufenbiel M, Nixon RA (2003) APP gene dosage modulates endosomal abnormalities of Alzheimer's disease in a segmental trisomy 16 mouse model of down syndrome. *J Neurosci* **23**, 6788-6792.

[18] Wisniewski K, Howe J, Williams DG, Wisniewski HM (1978) Precocious aging and dementia in patients with Down's syndrome. *Biol Psychiatry* **13**, 619-627.

[19] Cruts M, Theuns J, Van Broeckhoven C (2012) Locus-specific mutation databases for neurodegenerative brain diseases. *Hum Mutat* **33**, 1340-1344.

[20] Pastorino L, Lu KP (2006) Pathogenic mechanisms in Alzheimer's disease. *Eur J Pharmacol* **545**, 29-38.

[21] Jonsson T, Atwal JK, Steinberg S, Snaedal J, Jonsson PV, Bjornsson S, Stefansson H, Sulem P, Gudbjartsson D, Maloney J, Hoyte K, Gustafson A, Liu Y, Lu Y, Bhangale T, Graham RR, Huttenlocher J, Bjornsdottir G, Andreassen OA, Jonsson EG, Palotie A, Behrens TW, Magnusson OT, Kong A, Thorsteinsdottir U, Watts RJ, Stefansson K (2012) A mutation in APP protects against Alzheimer's disease and age-related cognitive decline. *Nature* **488**, 96-99.

[22] Corder EH, Saunders AM, Risch NJ, Strittmatter WJ, Schmechel DE, Gaskell PC Jr, Rimmler JB, Locke PA, Conneally PM, Schmader KE, Small GW, Roses AD, Haines JL, Pericak-Vance MA (1994) Protective effect of apolipoprotein E type 2 allele for late onset Alzheimer disease. *Nat Genet* **7**, 180-184.

[23] Serrano-Pozo A, Qian J, Monsell SE, Betensky RA, Hyman BT (2015) APOEepsilon2 is associated with milder clinical and pathological Alzheimer disease. *Ann Neurol* **77**, 917-929.

[24] Luo Y, Bolon B, Kahn S, Bennett BD, Babu-Khan S, Denis P, Fan W, Kha H, Zhang J, Gong Y, Martin L, Louis JC,

Yan Q, Richards WG, Citron M, Vassar R (2001) Mice deficient in BACE1, the Alzheimer's beta-secretase, have normal phenotype and abolished beta-amyloid generation. *Nat Neurosci* **4**, 231-232.

[25] Lee MS, Kao SC, Lemere CA, Xia W, Tseng HC, Zhou Y, Neve R, Ahlijanian MK, Tsai LH (2003) APP processing is regulated by cytoplasmic phosphorylation. *J Cell Biol* **163**, 83-95.

[26] Chang KA, Kim HS, Ha TY, Ha JW, Shin KY, Jeong YH, Lee JP, Park CH, Kim S, Baik TK, Suh YH (2006) Phosphorylation of amyloid precursor protein (APP) at Thr668 regulates the nuclear translocation of the APP intracellular domain and induces neurodegeneration. *Mol Cell Biol* **26**, 4327-4338.

[27] Pastorino L, Sun A, Lu PJ, Zhou XZ, Balastik M, Finn G, Wulf G, Lim J, Li SH, Li X, Xia W, Nicholson LK, Lu KP (2006) The prolyl isomerase Pin1 regulates amyloid precursor protein processing and amyloid-beta production. *Nature* **440**, 528-534.

[28] Ramelot TA, Gentile LN, Nicholson LK (2000) Transient structure of the amyloid precursor protein cytoplasmic tail indicates preordering of structure for binding to cytosolic factors. *Biochemistry* **39**, 2714-2725.

[29] Ramelot TA, Nicholson LK (2001) Phosphorylation-induced structural changes in the amyloid precursor protein cytoplasmic tail detected by NMR. *J Mol Biol* **307**, 871-884.

[30] De S, Greenwood AI, Rogals MJ, Kovrigin EL, Lu KP, Nicholson LK (2012) Complete thermodynamic and kinetic characterization of the isomer-specific interaction between Pin1-WW domain and the amyloid precursor protein cytoplasmic tail phosphorylated at Thr668. *Biochemistry* **51**, 8583-8596.

[31] Greenwood AI, Rogals MJ, De S, Lu KP, Kovrigin EL, Nicholson LK (2011) Complete determination of the Pin1 catalytic domain thermodynamic cycle by NMR lineshape analysis. *J Biomol NMR* **51**, 21-34.

[32] Ma SL, Pastorino L, Zhou XZ, Lu KP (2012) Prolyl isomerase Pin1 promotes amyloid precursor protein (APP) turnover by inhibiting glycogen synthase kinase-3beta (GSK3beta) activity: Novel mechanism for Pin1 to protect against Alzheimer disease. *J Biol Chem* **287**, 6969-6973.

[33] Southern PJ, Berg P (1982) Transformation of mammalian cells to antibiotic resistance with a bacterial gene under control of the SV40 early region promoter. *J Mol Appl Genet* **1**, 327-341.

[34] Thajudeen H, Park K, Moon S-S, Hong IS (2010) An efficient green synthesis of proline-based cyclic dipeptides under water-mediated catalyst-free conditions. *Tetrahedron Lett* **51**, 1303-1305.

[35] Estiarte MA, Diez A, Rubiralta M, Jackson RFW (2001) Synthesis of a 3-aminopiperidin-2,5-dione as a conformationally constrained surrogate of the Ala-Gly dipeptide. *Tetrahedron* **57**, 157-161.

[36] Zhao S, Etzkorn FA (2007) A phosphorylated prodrug for the inhibition of Pin1. *Bioorg Med Chem Lett* **17**, 6615-6618.

[37] Rivero-Gutiérrez B, Anzola A, Martínez-Augustin O, de Medina FS (2014) Stain-free detection as loading control alternative to Ponceau and housekeeping protein immunodetection in Western blotting. *Anal Biochem* **467**, 1-3.

[38] Laemmli UK (1970) Cleavage of structural proteins during the assembly of the head of bacteriophage T4. *Nature* **227**, 680-685.

[39] Towbin H, Staehelin T, Gordon J (1979) Electrophoretic transfer of proteins from polyacrylamide gels to nitrocellulose sheets: Procedure and some applications. *Proc Natl Acad Sci U S A* **76**, 4350-4354.

[40] Rosen RF, Tomidokoro Y, Ghiso JA, Walker LC (2010) SDS-PAGE/immunoblot detection of Abeta multimers in human cortical tissue homogenates using antigen-epitope retrieval. *J Vis Exp* (38), e1916, doi:10.3791/1916

[41] Winter D, Steen H (2011) Optimization of cell lysis and protein digestion protocols for the analysis of HeLa S3 cells by LC-MS/MS. *Proteomics* **11**, 4726-4730.

[42] Sebaugh JL (2011) Guidelines for accurate EC50/IC50 estimation. *Pharm Stat* **10**, 128-134.

[43] Wolfe MS, Xia W, Ostaszewski BL, Diehl TS, Kimberly WT, Selkoe DJ (1999) Two transmembrane aspartates in presenilin-1 required for presenilin endoproteolysis and gamma-secretase activity. *Nature* **398**, 513-517.

[44] Jager S, Leuchtenberger S, Martin A, Czirr E, Wesselowski J, Dieckmann M, Waldron E, Korth C, Koo EH, Heneka M, Weggen S, Pietrzik CU (2009) Alpha-secretase mediated conversion of the amyloid precursor protein derived membrane stub C99 to C83 limits Abeta generation. *J Neurochem* **111**, 1369-1382.

[45] Bustamante HA, Rivera-Dictter A, Cavieres VA, Muñoz VC, González A, Lin Y, Mardones GA, Burgos PV (2013) Turnover of C99 is controlled by a crosstalk between ERAD and ubiquitin-independent lysosomal degradation in human neuroglioma cells. *PLoS One* **8**, e83096.

[46] Farzan M, Schnitzler CE, Vasilieva N, Leung D, Choe H (2000) BACE2, a β-secretase homolog, cleaves at the β site and within the amyloid-β region of the amyloid-β precursor protein. *Proc Natl Acad Sci U S A* **97**, 9712-9717.

[47] Li Y, Zhou W, Tong Y, He G, Song W (2006) Control of APP processing and Aβ generation level by BACE1 enzymatic activity and transcription. *FASEB J* **20**, 285-292.

[48] Nikolaev A, McLaughlin T, O'Leary DDM, Tessier-Lavigne M (2009) APP binds DR6 to trigger axon pruning and neuron death via distinct caspases. *Nature* **457**, 981-989.

[49] Bodendorf U, Danner S, Fischer F, Stefani M, Sturchler-Pierrat C, Wiederhold KH, Staufenbiel M, Paganetti P (2002) Expression of human beta-secretase in the mouse brain increases the steady-state level of beta-amyloid. *J Neurochem* **80**, 799-806.

[50] Arnstein P, Taylor DO, Nelson-Rees WA, Huebner RJ, Lennette EH (1974) Propagation of human tumors in antithymocyte serum-treated mice. *J Natl Cancer Inst* **52**, 71-84.

[51] Day RS, 3rd, Ziolkowski CH (1979) Human brain tumour cell strains with deficient host-cell reactivation of N-methyl-N'-nitro-N-nitrosoguanidine-damaged adenovirus 5. *Nature* **279**, 797-799.

[52] Abisambra JF, Fiorelli T, Padmanabhan J, Neame P, Wefes I, Potter H (2010) LDLR expression and localization are altered in mouse and human cell culture models of Alzheimer's disease. *PLoS One* **5**, e8556.

[53] Asai M, Iwata N, Yoshikawa A, Aizaki Y, Ishiura S, Saido TC, Maruyama K (2007) Berberine alters the processing of Alzheimer's amyloid precursor protein to decrease Abeta secretion. *Biochem Biophys Res Commun* **352**, 498-502.

[54] Crestini A, Piscopo P, Iazeolla M, Albani D, Rivabene R, Forloni G, Confaloni A (2011) Rosuvastatin and thapsigargin modulate gamma-secretase gene expression and APP processing in a human neuroglioma model. *J Mol Neurosci* **43**, 461-469.

[55] Dickey CA, Ash P, Klosak N, Lee WC, Petrucelli L, Hutton M, Eckman CB (2006) Pharmacologic reductions of total tau levels; implications for the role of microtubule dynamics in regulating tau expression. *Mol Neurodegener* **1**, 6.

[56] Kang J, Muller-Hill B (1990) Differential splicing of Alzheimer's disease amyloid A4 precursor RNA in rat tissues: PreA4(695) mRNA is predominantly produced in rat and human brain. *Biochem Biophys Res Commun* **166**, 1192-1200.

[57] Belyaev ND, Kellett KA, Beckett C, Makova NZ, Revett TJ, Nalivaeva NN, Hooper NM, Turner AJ (2010) The transcriptionally active amyloid precursor protein (APP) intracellular domain is preferentially produced from the 695 isoform of APP in a beta-secretase-dependent pathway. *J Biol Chem* **285**, 41443-41454.

[58] Tomita T, Iwatsubo T (2004) The inhibition of gamma-secretase as a therapeutic approach to Alzheimer's disease. *Drug News Perspect* **17**, 321-325.

[59] Farquhar D, Chen R, Khan S (1995) 5'-[4-(Pivaloyloxy)-1,3,2-dioxaphosphorinan-2-yl]-2'-deoxy-5-fluorouridine: A membrane-permeating prodrug of 5-fluoro-2'-deoxyuridylic acid (FdUMP). *J Med Chem* **38**, 488-495.

[60] Citron M (2002) Beta-secretase as a target for the treatment of Alzheimer's disease. *J Neurosci Res* **70**, 373-379.

[61] Vassar R, Kuhn PH, Haass C, Kennedy ME, Rajendran L, Wong PC, Lichtenthaler SF (2014) Function, therapeutic potential and cell biology of BACE proteases: Current status and future prospects. *J Neurochem* **130**, 4-28.

[62] Castrillo JI, Oliver SG (2016) Alzheimer's as a systems-level disease involving the interplay of multiple cellular networks. *Methods Mol Biol* **1303**, 3-48.

[63] Jiang S, Li Y, Zhang X, Bu G, Xu H, Zhang YW (2014) Trafficking regulation of proteins in Alzheimer's disease. *Mol Neurodegener* **9**, 6.

[64] Sannerud R, Declerck I, Peric A, Raemaekers T, Menendez G, Zhou L, Veerle B, Coen K, Munck S, De Strooper B, Schiavo G, Annaert W (2011) ADP ribosylation factor 6 (ARF6) controls amyloid precursor protein (APP) processing by mediating the endosomal sorting of BACE1. *Proc Natl Acad Sci U S A* **108**, E559-568.

[65] Annaert W (2012) Sorting out the cell biology of Alzheimer's disease: Focus on BACE1 and APP. *Mol Neurodegener* **7**, 1-2.

[66] Kalvodova L, Kahya N, Schwille P, Ehehalt R, Verkade P, Drechsel D, Simons K (2005) Lipids as modulators of proteolytic activity of BACE: Involvement of cholesterol, glycosphingolipids, and anionic phospholipids *in vitro*. *J Biol Chem* **280**, 36815-36823.

[67] van der Kant R, Goldstein LS (2015) Cellular functions of the amyloid precursor protein from development to dementia. *Dev Cell* **32**, 502-515.

[68] Vassar R, Bennett BD, Babu-Khan S, Kahn S, Mendiaz EA, Denis P, Teplow DB, Ross S, Amarante P, Loeloff R, Luo Y, Fisher S, Fuller J, Edenson S, Lile J, Jarosinski MA, Biere AL, Curran E, Burgess T, Louis JC, Collins F, Treanor J, Rogers G, Citron M (1999) Beta-secretase cleavage of Alzheimer's amyloid precursor protein by the transmembrane aspartic protease BACE. *Science* **286**, 735-741.

[69] Hosaka A, Araki W, Oda A, Tomidokoro Y, Tamaoka A (2013) Statins reduce amyloid beta-peptide production by modulating amyloid precursor protein maturation and phosphorylation through a cholesterol-independent mechanism in cultured neurons. *Neurochem Res* **38**, 589-600.

[70] Zhu Z, Li C, Wang X, Yang Z, Chen J, Hu L, Jiang H, Shen X (2010) 2,2',4'-trihydroxychalcone from Glycyrrhiza glabra as a new specific BACE1 inhibitor efficiently ameliorates memory impairment in mice. *J Neurochem* **114**, 374-385.

[71] Adlard PA, Cherny RA, Finkelstein DI, Gautier E, Robb E, Cortes M, Volitakis I, Liu X, Smith JP, Perez K, Laughton K, Li QX, Charman SA, Nicolazzo JA, Wilkins S, Deleva K, Lynch T, Kok G, Ritchie CW, Tanzi RE, Cappai R, Masters CL, Barnham KJ, Bush AI (2008) Rapid restoration of cognition in Alzheimer's transgenic mice with 8-hydroxy quinoline analogs is associated with decreased interstitial Abeta. *Neuron* **59**, 43-55.

[72] Kupershmidt L, Amit T, Bar-Am O, Weinreb O, Youdim MB (2012) Multi-target, neuroprotective and neurorestorative M30 improves cognitive impairment and reduces Alzheimer's-like neuropathology and age-related alterations in mice. *Mol Neurobiol* **46**, 217-220.

[73] Matlack KE, Tardiff DF, Narayan P, Hamamichi S, Caldwell KA, Caldwell GA, Lindquist S (2014) Clioquinol promotes the degradation of metal-dependent amyloid-beta (Abeta) oligomers to restore endocytosis and ameliorate Abeta toxicity. *Proc Natl Acad Sci U S A* **111**, 4013-4018.

[74] Wang Y, Branicky R, Stepanyan Z, Carroll M, Guimond MP, Hihi A, Hayes S, McBride K, Hekimi S (2009) The anti-neurodegeneration drug clioquinol inhibits the aging-associated protein CLK-1. *J Biol Chem* **284**, 314-323.

[75] White AR, Du T, Laughton KM, Volitakis I, Sharples RA, Xilinas ME, Hoke DE, Holsinger RM, Evin G, Cherny RA, Hill AF, Barnham KJ, Li QX, Bush AI, Masters CL (2006) Degradation of the Alzheimer disease amyloid beta-peptide by metal-dependent up-regulation of metalloprotease activity. *J Biol Chem* **281**, 17670-17680.

[76] Berra E, Benizri E, Ginouves A, Volmat V, Roux D, Pouyssegur J (2003) HIF prolyl-hydroxylase 2 is the key oxygen sensor setting low steady-state levels of HIF-1alpha in normoxia. *EMBO J* **22**, 4082-4090.

[77] Choi SM, Choi KO, Park YK, Cho H, Yang EG, Park H (2006) Clioquinol, a Cu(II)/Zn(II) chelator, inhibits both ubiquitination and asparagine hydroxylation of hypoxia-inducible factor-1alpha, leading to expression of vascular endothelial growth factor and erythropoietin in normoxic cells. *J Biol Chem* **281**, 34056-34063.

[78] Hewitson KS, McNeill LA, Schofield CJ (2004) Modulating the hypoxia-inducible factor signaling pathway: Applications from cardiovascular disease to cancer. *Curr Pharm Des* **10**, 821-833.

[79] Moon H, Han S, Park H, Choe J (2010) Crystal structures of human FIH-1 in complex with quinol family inhibitors. *Mol Cells* **29**, 471-474.

[80] Lando D, Peet DJ, Gorman JJ, Whelan DA, Whitelaw ML, Bruick RK (2002) FIH-1 is an asparaginyl hydroxylase enzyme that regulates the transcriptional activity of hypoxia-inducible factor. *Genes Dev* **16**, 1466-1471.

[81] Liu W, Shen SM, Zhao XY, Chen GQ (2012) Targeted genes and interacting proteins of hypoxia inducible factor-1. *Int J Biochem Mol Biol* **3**, 165-178.

[82] Bae MK, Ahn MY, Jeong JW, Bae MH, Lee YM, Bae SK, Park JW, Kim KR, Kim KW (2002) Jab1 interacts directly with HIF-1alpha and regulates its stability. *J Biol Chem* **277**, 9-12.